

# Dissecting the Electrostatic Interactions and pH-Dependent Activity of a Family 11 Glycosidase<sup>†,‡</sup>

Manish D. Joshi,<sup>§,||</sup> Gary Sidhu,<sup>§</sup> Jens E. Nielsen,<sup>⊥</sup> Gary D. Brayer,<sup>§</sup> Stephen G. Withers,<sup>§,#</sup> and Lawrence P. McIntosh<sup>\*,§,#,○</sup>

Department of Biochemistry and Molecular Biology, Department of Chemistry, and The Biotechnology Laboratory, University of British Columbia, Vancouver, British Columbia, Canada V6T 1Z3, and European Molecular Biology Laboratory, Heidelberg, Germany 69117

Received March 15, 2001; Revised Manuscript Received June 19, 2001

**ABSTRACT:** Previous studies of the low molecular mass family 11 xylanase from *Bacillus circulans* show that the ionization state of the nucleophile (Glu78, pK<sub>a</sub> 4.6) and the acid/base catalyst (Glu172, pK<sub>a</sub> 6.7) gives rise to its pH-dependent activity profile. Inspection of the crystal structure of BCX reveals that Glu78 and Glu172 are in very similar environments and are surrounded by several chemically equivalent and highly conserved active site residues. Hence, there are no obvious reasons why their apparent pK<sub>a</sub> values are different. To address this question, a mutagenic approach was implemented to determine what features establish the pK<sub>a</sub> values (measured directly by <sup>13</sup>C NMR and indirectly by pH-dependent activity profiles) of these two catalytic carboxylic acids. Analysis of several BCX variants indicates that the ionized form of Glu78 is preferentially stabilized over that of Glu172 in part by stronger hydrogen bonds contributed by two well-ordered residues, namely, Tyr69 and Gln127. In addition, theoretical pK<sub>a</sub> calculations show that Glu78 has a lower pK<sub>a</sub> value than Glu172 due to a smaller desolvation energy and more favorable background interactions with permanent partial charges and ionizable groups within the protein. The pK<sub>a</sub> value of Glu172 is in turn elevated due to electrostatic repulsion from the negatively charged glutamate at position 78. The results also indicate that all of the conserved active site residues act concertedly in establishing the pK<sub>a</sub> values of Glu78 and Glu172, with no particular residue being singly more important than any of the others. In general, residues that contribute positive charges and hydrogen bonds serve to lower the pK<sub>a</sub> values of Glu78 and Glu172. The degree to which a hydrogen bond lowers a pK<sub>a</sub> value is largely dependent on the length of the hydrogen bond (shorter bonds lower pK<sub>a</sub> values more) and the chemical nature of the donor (COOH > OH > CONH<sub>2</sub>). In contrast, neighboring carboxyl groups can either lower or raise the pK<sub>a</sub> values of the catalytic glutamic acids depending upon the electrostatic linkage of the ionization constants of the residues involved in the interaction. While the pH optimum of BCX can be shifted from -1.1 to +0.6 pH units by mutating neighboring residues within the active site, activity is usually compromised due to the loss of important ground and/or transition state interactions. These results suggest that the pH optima of an enzyme might be best engineered by making strategic amino acid substitutions, at positions outside of the “core” active site, that electrostatically influence catalytic residues without perturbing their immediate structural environment.

Enzymes catalyze virtually all biochemical reactions in a bewildering array of organisms and often under extremes of environmental conditions. Remarkably, this can be carried out using a rather limited repertoire of amino acids that serve as nucleophiles, electrophiles, and general acids and bases. Clearly, enzyme structures have evolved in part to modulate

the physicochemical properties of these amino acids, as required for catalysis of a particular reaction under a given set of conditions. Since these catalytic amino acids generally have ionizable side chains, one critical property is their precise pK<sub>a</sub> value within the context of the native enzyme.

<sup>†</sup> This work was funded by the Government of Canada's Network of Centres of Excellence Program supported by the Medical Research Council (MRC) and the Natural Sciences and Engineering Research Council (NSERC) through the Protein Engineering Network of Centres of Excellence (PENCE Inc.). L.P.M. acknowledges the Alexander von Humboldt Foundation for support of a sabbatical leave with Dr. M. Nilges at The European Molecular Biology Laboratory, Heidelberg, Germany, and the Canadian Institutes of Health Research for a Scientist Award.

<sup>‡</sup> Coordinates for the structures described in this work have been deposited in the Research Collaboratory for Structural Bioinformatics (RCSB) Protein Data Bank (PDB) (accession numbers 1HV0 and 1HV1).

\* Address correspondence to this author at the Department of Biochemistry and Molecular Biology, University of British Columbia, 2146 Health Sciences Mall, Vancouver, BC, Canada V6T 1Z3. Tel: (604) 822-3341. Fax: (604) 822-5227. E-mail: mcintosh@otter.biochem.ubc.ca.

<sup>§</sup> Department of Biochemistry and Molecular Biology, University of British Columbia.

<sup>||</sup> Present address: Ontario Cancer Institute/Princess Margaret Hospital, Division of Molecular and Structural Biology, University of Toronto, Department of Medical Biophysics, Toronto, ON, Canada M5G 2M9.

<sup>⊥</sup> European Molecular Biology Laboratory.

<sup>#</sup> Department of Chemistry, University of British Columbia.

<sup>○</sup> The Biotechnology Laboratory, University of British Columbia.

For example, all low molecular mass xylanases use the same configuration of two catalytic glutamic acids to hydrolyze xylan. The  $pK_a$  values of these two residues, however, differ considerably within a given enzyme as one must be deprotonated to serve as a nucleophile, while the other must be protonated to function as a general acid. In addition, the relative  $pK_a$  values of these catalytic residues must be shifted between individual members of this family as some xylanases function optimally under acidic conditions, whereas others function under more alkaline pH values. Accordingly, a major challenge in the field of enzymology is to delineate experimentally the parameters that establish the  $pK_a$  values of ionizable groups in proteins and protein complexes. Knowledge of these factors can be applied to rationally engineer the pH optima of enzymes for use in biotechnology, as well as to improve their pH-dependent stability. Furthermore, studies that provide direct experimental information about structural and functional electrostatic interactions in proteins will also aid in the development and refinement of suitable algorithms for the theoretical prediction of the  $pK_a$  values of their constituent ionizable groups.

The low molecular mass endo- $\beta$ -(1,4)-xylanase from *Bacillus circulans* (BCX)<sup>1</sup> (1, 2) provides an excellent model system to study the pH-dependent activity of retaining glycosidases. This 20.4 kDa enzyme has been extensively characterized kinetically (3–6) and structurally (3, 7, 8) in both its free and covalent glycosyl enzyme–intermediate states. In addition, the NMR spectrum of BCX has been assigned (9), and the  $pK_a$  values of all of its carboxyl (6, 10) and imidazole (11) groups have been determined.

BCX, like all family 11 glycosidase members (12), hydrolyzes xylosidic substrates with net retention of anomeric configuration. This proceeds via a double-displacement mechanism in which a covalent intermediate is formed in the glycosylation step and subsequently hydrolyzed in the deglycosylation step (13–15) (Figure 1). Previous studies have determined that, during the glycosylation reaction, Glu78 serves as a nucleophile and thus must initially be negatively charged, whereas Glu172 functions as a general acid and hence must be protonated (6, 7, 16). Consistent with their catalytic roles, the  $pK_a$  values of Glu78 and Glu172, measured directly using <sup>13</sup>C NMR spectroscopy, are 4.6 and 6.7, respectively. These values are in close agreement with those determined from the bell-shaped pH–activity profile of this enzyme and show that the ionization states of Glu78 and Glu172 determine that BCX functions optimally at pH 5.7 (6).

The double-displacement mechanism of BCX necessitates that Glu172 plays a dual catalytic role as a general acid in the first step and as a general base in the second. This requirement places specific demands on the ionization state of Glu172. Remarkably, when the  $pK_a$  of Glu172 is measured in a trapped covalent glycosyl-enzyme intermediate, its value drops to 4.2, such that, at the pH optimum of BCX, this glutamate is now negatively charged. The  $pK_a$  of Glu172 thus “cycles” to match its dual catalytic role (6). A similarly low  $pK_a$  (4.2) was measured for Glu172 in a BCX variant where Glu78 was substituted with a glutamine. This large decrease in  $pK_a$  of  $\sim$ 2.5 units is consistent with the role of Glu172 as a general base catalyst in the deglycosylation step and appears to be a consequence of reduced electrostatic repulsion due to neutralization of Glu78, augmented by subtle conformational changes in the protein. Hence, this phenomenon is intrinsic to the retaining mechanism of glycosidases, with the predominant driving force for  $pK_a$  cycling being the change in the ionization state of Glu78 from a negatively charged nucleophile to a neutral glycosylated residue during the double-displacement reaction.

A major goal of this study of BCX is to delineate the factors that establish the exact  $pK_a$  values of these two catalytic glutamic acid residues. As expected, crystallographic studies of BCX reveal that Glu78 and Glu172 are surrounded by several highly conserved residues within the active site of the enzyme (8). However, upon closer inspection, Glu78 and Glu172 are both found to be hydrogen bonded to primary amides (Gln127 and Asn35, respectively) and phenolic oxygens (Tyr69 and Tyr80, respectively), and they are approximately equidistant from the same positively charged arginine (Arg112). Furthermore, both catalytic residues are in similar environments of secondary structure and exhibit comparable accessibilities to the solvent (2). Thus, there is no obvious reason as to why the microscopic  $pK_a$  values of these two glutamic acids differ such that Glu78 ionizes preferentially before Glu172 with increasing pH (6; Figure S1, Supporting Information). To help to answer this question, we have undertaken a systematic mutagenic study in order to determine the effects that specific hydrogen-bonding and electrostatic interactions, contributed by conserved neighboring residues, have upon the  $pK_a$  values of Glu78 and Glu172 and hence the pH-dependent activity of BCX.

In this study, we report the kinetic, NMR spectroscopic, and X-ray crystallographic analyses of several BCX variants containing substitutions of active site residues. Proteins were characterized kinetically in both the pre-steady-state and steady-state phases of hydrolysis. In particular, the second-order rate constants  $k_{cat}/K_m$  for hydrolysis of a xylobiosyl derivative were measured for all of the proteins as a function of pH. From the resultant bell-shaped activity profiles, the pH optimum of each variant, as well as the apparent  $pK_a$  values of Glu78 and Glu172, could be extracted and compared to those of the wild-type enzyme. In parallel, NMR spectroscopy was utilized to measure directly the  $pK_a$  values of these two catalytic residues in each mutant protein. Where possible, X-ray crystallographic structures of mutant xylanases were solved to provide additional structural information. The structure of WT BCX was also determined under acidic conditions to assess the extent of pH-dependent conformational changes, which may influence the activity of the enzyme. Finally, the  $pK_a$  values of the catalytic

<sup>1</sup> Abbreviations: BCX, *Bacillus circulans* xylanase; BSA, bovine serum albumin; CHES, 2-(*N*-cyclohexylamino)ethanesulfonic acid;  $\delta\Delta$ , the magnitude and direction of the chemical shift change upon deprotonation of the listed residue; 2,5-DNPX<sub>2</sub>, 2,5-dinitrophenyl  $\beta$ -xylobioside; DNP2FXb, 2,4-dinitrophenyl 2-deoxy-2-fluoro- $\beta$ -xylobioside; DSS, 3-(trimethylsilyl)-1-propanesulfonic acid; 2FXb, 2-deoxy-2-fluoro- $\beta$ -xylobioside; HEPES, 4-(2-hydroxyethyl)-1-piperazineethanesulfonic acid; IPTG, isopropyl  $\beta$ -D-thiogalactopyranoside; MES, 2-(*N*-morpholino)ethanesulfonic acid; NMR, nuclear magnetic resonance; ONPX<sub>2</sub>, *o*-nitrophenyl  $\beta$ -xylobioside; pH\*, the measured pH without correction for isotope effect; rms, root mean square; SDS–PAGE, sodium dodecyl sulfate–polyacrylamide gel electrophoresis; S<sub>N</sub>2, biomolecular nucleophilic substitution; WT, wild type; WT-2FXb, 2-deoxy-2-fluoro- $\beta$ -xylobioside covalent glycosyl-enzyme intermediate of wild-type *B. circulans* xylanase; Xb, xylobiose; WT-Xb, noncovalent complex of wild-type *B. circulans* xylanase with xylobiose.

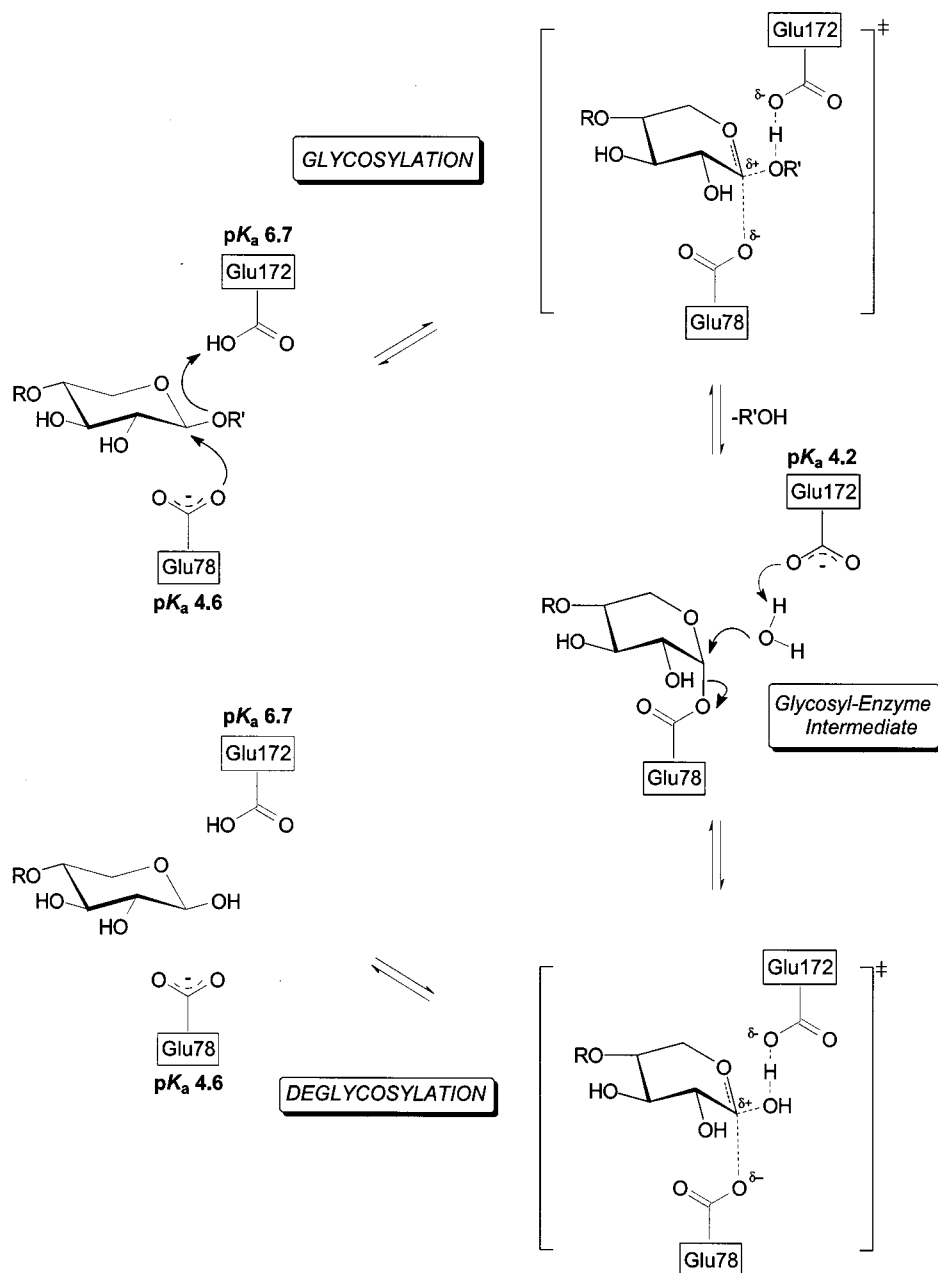


FIGURE 1: The double-displacement anomer-retaining mechanism employed by BCX involves two distinct steps. In the glycosylation step, Glu78 functions as a nucleophile ( $pK_a$  4.6) and attacks the glycosidic bond of the  $\beta$ -(1,4)-linked xylose polymer while Glu172 functions as a general acid ( $pK_a$  6.7) and donates a proton to the departing aglycon (6). In the subsequent deglycosylation step, the glycosyl-enzyme intermediate [with the proximal saccharide distorted in the  ${}^2_5B$  conformation (7)] is hydrolyzed with the assistance of Glu172 ( $pK_a$  4.2), which now functions as a general base. Glu78 and Glu172 are shown in their predominant ionization states at the pH optimum of  $\sim 5.7$  for BCX ( $R, R' = \text{xylose}_n$ ).

glutamic acids were calculated theoretically in order to help to dissect the factors contributing to the differences observed between the WT and mutant enzymes. The amenability of BCX to being studied by a number of techniques has afforded us this unique opportunity to characterize its pH-dependent activity in great detail.

## EXPERIMENTAL PROCEDURES

**Cloning, Mutagenesis, and Protein Expression.** The synthetic gene encoding BCX was cloned into the pCW plasmid system under control of an inducible *tac* promoter, as described previously (1, 6, 8). To create the genes encoding the N35A, Y69F, Y80F, R112N, and Q127A variants of

BCX, site-directed mutagenesis was carried out as described previously (8) using the Kunkel method (17). The Quick-Change site-directed mutagenesis kit (Stratagene Cloning Systems, La Jolla, CA) was used to create the gene encoding Q127E BCX. All other recombinant DNA procedures, such as plasmid isolation and purification, were performed as recommended by the manufacturers. After the sequences were confirmed by automated DNA sequencing, the mutated plasmids were transformed into an appropriate bacterial *Escherichia coli* strain using electroporation or calcium chloride-heat shock.

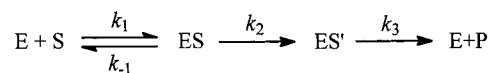
Proteins used for kinetic studies were expressed in *E. coli* strain BL21 ( $\lambda$ DE3) or 594 grown in TYP medium at 37

°C until the time of induction ( $OD_{600} = 0.5-0.6$ ) and thereafter at 30 °C until the cells were harvested 16 h later. Protein expression was induced by addition of IPTG to a final concentration of 0.75 mM. Purification was performed as described previously using SP-Sepharose ion-exchange chromatography followed by Sephacryl S-100 HR size exclusion chromatography (Pharmacia Biotech, Inc.) (1). Fresh column material was used for different proteins to prevent any possible cross-contamination. Proteins were purified to >95% homogeneity as judged by SDS-PAGE and Coomassie staining. Further characterization was performed using a Perkin-Elmer Sciex API III electrospray mass spectrometer with the following results: N35A, observed  $20\,358 \pm 3.5$  Da (expected 20 353 Da); Y69F, observed  $20\,385 \pm 4.5$  Da (expected 20 380 Da); Y80F, observed  $20\,385 \pm 4.5$  Da (expected 20 380 Da); R112N, observed  $20\,359 \pm 3.5$  Da (expected 20 354 Da); Q127A, observed  $20\,344 \pm 4.0$  Da (expected 20 339 Da); and Q127E, observed  $20\,400 \pm 3.5$  Da (expected 20 402 Da).

BCX mutant proteins,  $^{13}\text{C}$ -enriched in the side chain  $\delta$ -carbonyl of the glutamate and glutamine residues, were prepared as described previously (6). Bacteria were grown in a synthetic medium (6, 18, 19) containing 275–325 mg/L 99% L- $[\delta\text{-}^{13}\text{C}]$ glutamate (Tracer Technology, Cambridge, MA). The isotopically labeled proteins were expressed and purified as above, except that the size exclusion chromatography step was not performed in order to maximize yield. The  $[\delta\text{-}^{13}\text{C}]$ Glu- and  $[\delta\text{-}^{13}\text{C}]$ Gln-enriched xylanases were purified to >90% homogeneity as judged by SDS-PAGE and Coomassie Blue staining. Further characterization was performed using electrospray mass spectrometry, yielding the following values: N35A, observed  $20\,351 \pm 3.5$  Da (expected 20 360 Da); Y69F, observed  $20\,391 \pm 2.0$  Da (expected 20 387 Da); Y80F, observed  $20\,387 \pm 2.0$  Da (expected 20 387 Da); R112N, observed  $20\,362 \pm 2.4$  Da (expected 20 361 Da); Q127A, observed  $20\,346 \pm 3.6$  Da (expected 20 346 Da); and Q127E, observed  $20\,408 \pm 3.2$  Da (expected 20 409 Da). The expected mass value was calculated assuming 100%  $^{13}\text{C}$  enrichment of seven residues. Deviations between the observed and expected molecular masses reflect isotopic dilution of the  $[\delta\text{-}^{13}\text{C}]$ glutamate.

**Enzyme Kinetics.** (i) *Steady-State Kinetics.* Two aryl  $\beta$ -xylobiosides were used as substrates in the assays described below: 2,5-dinitrophenyl  $\beta$ -xylobioside (2,5-DNPX<sub>2</sub>),  $\Delta\epsilon_{440\text{nm}} = 3.57 \text{ mM}^{-1} \text{ cm}^{-1}$  (where  $\Delta\epsilon$  is the difference in molar absorptivity between the phenol and its corresponding xylobioside at pH 6.0), and *o*-nitrophenyl  $\beta$ -xylobioside (ONPX<sub>2</sub>),  $\Delta\epsilon_{400\text{nm}} = 1.07 \text{ mM}^{-1} \text{ cm}^{-1}$ . All substrates were synthesized and characterized according to previously published procedures (5, 20). All other materials, unless otherwise stated, were obtained from the Sigma Chemical Co. Spectrophotometric assays were performed using either a Pye Unicam 8700 or UV4 UV-vis spectrophotometer, both equipped with a circulating water bath for temperature control. Assays were carried out in 200  $\mu\text{L}$  micro-black-walled quartz cuvettes with a 1 cm path length, according to methods described previously (5). The pH values of assay solutions were measured using a Corning G-P Micro Combo electrode. Steady-state kinetic data were fitted using the programs PlotData (TRIUMF, University of British Columbia) and GraFit (21).

Scheme 1



Assays to determine the Michaelis–Menten steady-state parameters,  $k_{\text{cat}}$  and  $K_{\text{m}}$ , utilized the appropriate aryl  $\beta$ -xylobioside substrate in 20 mM MES, 50 mM NaCl, and 0.1% BSA buffer (pH 6.0). Typically, substrate concentrations were varied from  $0.2K_{\text{m}}$  to  $5K_{\text{m}}$ . After a 15 min preincubation time at 40 °C, 10  $\mu\text{L}$  of enzyme at an appropriate concentration (20–70  $\mu\text{M}$  final) was added to 190  $\mu\text{L}$  of the assay solution. The initial rates of enzymatic hydrolysis of the aryl  $\beta$ -xylobiosides,  $v_0$ , were determined by monitoring the rate of phenol release at the appropriate wavelength in a continuous assay at 40 °C. Enzyme concentrations and reaction times were chosen such that less than 10% of the total substrate was hydrolyzed over the course of the measurement. Experimental rates measured at each given substrate concentration were nonlinear least squares fitted to the standard Michaelis–Menten expression (Scheme 1 and eqs 1–4, where  $k_2$  and  $k_3$  represent the glycosylation and deglycosylation steps, respectively, while ES and ES' are the noncovalent enzyme substrate and covalent glycosyl-enzyme intermediate, respectively) to obtain the parameters  $k_{\text{cat}}$  and  $K_{\text{m}}$ . Values of  $k_{\text{cat}}/K_{\text{m}}$  were determined from the slope of a Lineweaver–Burk plot.

$$v_0 = \frac{k_{\text{cat}}[\text{E}_\text{T}][\text{S}]}{K_{\text{m}} + [\text{S}]} \quad (1)$$

where

$$k_{\text{cat}} = \frac{k_2 k_3}{k_2 + k_3} \quad (2)$$

$$K_{\text{m}} = \left( \frac{k_{-1} + k_2}{k_1} \right) \left( \frac{k_3}{k_2 + k_3} \right) \quad (3)$$

and

$$K_{\text{d}} = \frac{k_{-1}}{k_1} \quad (4)$$

Errors are estimated to be 5–10% on the basis of the accuracy by which substrate and enzyme concentrations can be determined.

Assays used to determine the pH dependence of  $k_{\text{cat}}/K_{\text{m}}$  employed low concentrations of ONPX<sub>2</sub> substrate (0.35 mM), 50 mM NaCl, 0.1% BSA, and the appropriate buffer for a given pH range (pH 2–5, 20 mM succinate; pH 5–7, 20 mM MES; pH 7–8, 20 mM HEPES; pH 8–11, 20 mM CHES). After a 15 min preincubation time at 25 °C, the enzymatic reaction was initiated by addition of 10  $\mu\text{L}$  of enzyme (3  $\mu\text{M}$  final) to 190  $\mu\text{L}$  of the assay solution. Progress curves were followed by measuring the release of *o*-nitrophenolate at 400 nm versus time until at least 80% substrate depletion was observed. The pH of each assay solution was measured after completion of the reaction. An aliquot of the assay mix was then reassayed at pH 6.0 to confirm the stability of the enzyme compared to an aliquot of unassayed enzyme which had not been exposed to assay

conditions. Experimental data were fitted to a pseudo-first-order expression, which upon division by the enzyme concentration yielded  $k_{\text{cat}}/K_m$  values. This method obviated the need to correct for the variation of extinction coefficient of ONPX<sub>2</sub> with pH and eliminated any errors associated with the determination of substrate concentrations. The  $k_{\text{cat}}/K_m$  data were then plotted as a function of pH and fitted to a bell-shaped activity profile, described in eq 5, from which apparent  $\text{p}K_a$  values corresponding to the acidic ( $\text{p}K_{a1}$ ) and basic limbs ( $\text{p}K_{a2}$ ) were determined by nonlinear least-squares fitting. An error in these  $\text{p}K_a$  values of  $\pm 0.1$  pH units is estimated from the error in the pH measurements.

$$\left(\frac{k_{\text{cat}}}{K_m}\right)_{\text{obs}} = \left(\frac{k_{\text{cat}}}{K_m}\right)_{\text{max}} \left( \frac{1}{1 + \frac{10^{-\text{pH}}}{10^{-\text{p}K_{a1}}} + \frac{10^{-\text{p}K_{a2}}}{10^{-\text{pH}}}} \right) \quad (5)$$

(ii) *Pre-Steady-State Kinetics.* Pre-steady-state kinetic measurements were taken for mutant BCX proteins using a stopped-flow spectrophotometer (Olis RSM-1000) with a 2 cm cell path length and a circulating water bath, as described previously (22). The dead time of the instrument is 2.5 ms. Assays consisted of various amounts of 2,5-DNPX<sub>2</sub> substrate (0.30–2.20 mM) and enzyme (1–2  $\mu\text{M}$ ) in 10 mM MES and 25 mM NaCl buffer (pH 6.0) at 25 °C. The limited solubility of 2,5-DNPX<sub>2</sub> under the conditions described precluded assays containing higher concentrations of substrate. Phenolate release was monitored at 440 nm by collecting data at a rate of 1000 spectra per second over a 10 s time period. Pre-steady-state bursts were observed only for Y80F BCX. For this protein, the resulting time courses were fitted to an expression with an exponential term (pre-steady-state phase) and a linear term (steady-state phase) (eq 6). First-order rate constants for the exponential pre-steady-

$$A_{440}(t) = A(1 - e^{k_{\text{obs}}t}) + Bt + C \quad (6)$$

state phase ( $k_{\text{obs}}$ ) were then fitted to a linearized form of eq 7 that is valid in the absence of saturating conditions ( $[S] < K_d$ ) (eq 8) (22–24). The slope of this plot yielded subsequent values of  $k_2/K_d$ .

$$k_{\text{obs}} = k_3 + \frac{k_2[S]}{k_d + [S]} \quad (7)$$

$$k_{\text{obs}} = k_3 + \frac{k_2[S]}{k_d} \quad (8)$$

*NMR.* All NMR spectra were recorded using a Varian Unity spectrometer operating at 500 MHz for protons.

(i) *Titration Curves.* The  $[\delta\text{-}^{13}\text{C}]\text{Glu-}$  and  $[\delta\text{-}^{13}\text{C}]\text{Gln-}$  enriched BCX proteins were dialyzed or exchanged, using a microconcentration device, into 10 mM sodium phosphate and 10% D<sub>2</sub>O/90% H<sub>2</sub>O at  $\text{pH}^* \sim 6.0$  with a total sample volume of 2.0 mL. Initial sample concentrations were as follows: N35A, 1.27 mM; Y69F, 1.20 mM; Y80F, 1.45 mM; R112N, 0.75 mM; Q127A, 0.37 mM; and Q127E, 0.42 mM. Titration curves were generated by recording <sup>13</sup>C NMR spectra of  $[\delta\text{-}^{13}\text{C}]\text{Glu-}$  and  $[\delta\text{-}^{13}\text{C}]\text{Gln-}$  labeled xylanases as a function of  $\text{pH}^*$  at 25 °C and were processed as described previously (6). Chemical shifts were referenced to an external

sample of DSS at 0.00 ppm. Proteins were titrated using microliter aliquots of either 0.25–0.50 M HCl or NaOH. The  $\text{pH}^*$  of the sample was determined using a Corning G-P Micro Combo electrode. After measurement of the acidic limb of the titration curve, the protein was exchanged into neutral buffer using a microconcentrating device to remove any excess salt and to avoid aggregation resulting from the direct addition of a large quantity of base. Titration of the basic limb was then carried out. The sample was also centrifuged periodically to remove any precipitate that formed over the course of the titration. Individual  $\delta$ -carbon resonances of glutamate and glutamine side chains of mutant xylanase proteins were assigned on the basis of previous analysis of the WT spectra (6, 9). Macroscopic  $\text{p}K_a$  values were determined by nonlinear least-squares fitting of the observed data to models involving one, two, or three sequential macroscopic ionizations (eqs 9–11) (25) using the program, PlotData (TRIUMF, University of British Columbia).

$$\delta_{\text{obs}} = \frac{\delta_a 10^{-\text{pH}} + \delta_b 10^{-\text{p}K_a}}{10^{-\text{pH}} + 10^{-\text{p}K_a}} \quad (9)$$

$$\delta_{\text{obs}} = \frac{\delta_a 10^{-2\text{pH}} + \delta_b 10^{-(\text{pH}+\text{p}K_{a1})} + \delta_c 10^{-(\text{p}K_{a1}+\text{p}K_{a2})}}{10^{-2\text{pH}} + 10^{-(\text{pH}+\text{p}K_{a1})} + 10^{-(\text{p}K_{a1}+\text{p}K_{a2})}} \quad (10)$$

$$\delta_{\text{obs}} = (\delta_a 10^{-3\text{pH}} + \delta_b 10^{-(\text{p}K_{a3}+2\text{pH})} + \delta_c 10^{-(\text{p}K_{a2}+\text{p}K_{a3}+\text{pH})} + \delta_d 10^{-(\text{p}K_{a1}+\text{p}K_{a2}+\text{p}K_{a3})}) / (10^{-3\text{pH}} + 10^{-(\text{p}K_{a3}+2\text{pH})} + 10^{-(\text{p}K_{a2}+\text{p}K_{a3}+\text{pH})} + 10^{-(\text{p}K_{a1}+\text{p}K_{a2}+\text{p}K_{a3})}) \quad (11)$$

Here,  $\delta_{\text{obs}}$  is the chemical shift of the residue being monitored and  $\delta_i$  represents its chemical shift in each ionization state of the enzyme. Selection of the appropriate model was based on the criteria of using the minimal number of ionization events to adequately fit the observed titration data as judged by a visual comparison of the observed and calculated plots of  $\delta_{\text{obs}}$  versus  $\text{pH}^*$ . The error of the pH measurements and hence resulting  $\text{p}K_a$  values is estimated to be  $\pm 0.1$  units.

*X-ray Crystallography.* Crystals of mutant BCX proteins were grown at pH 7.5 in 17–20% (NH<sub>4</sub>)<sub>2</sub>SO<sub>4</sub>, 10 mM NaCl, and 40 mM Tris-HCl as previously described for the WT enzyme (7). The crystals of WT BCX at acidic pH values were prepared by further soaking those grown at pH 7.5 in 1.0 M sodium citrate buffer at pH 5.5 or pH 4.0 for approximately 4 h. Diffraction data for each mutant were collected from a single crystal on a Rigaku R-AXIS IIC imaging plate area detector system using Cu K $\alpha$  radiation supplied by a Rigaku RU300 rotating anode generator operating at 50 kV and 100 mA. Each diffraction data frame was exposed for 20 min, during which time the crystal was oscillated through 1.2°. Intensity data were integrated, scaled, and reduced to structure factor amplitudes with the HKL suite of programs (26) (Table 1). Because all types of crystals retained unit cells isomorphous to WT BCX, the published structure of the parent enzyme (8), with the residue at the site of mutation truncated to alanine, was used as the starting model in each case. These models were subjected to rigid body, simulated annealing, positional, and individual isotropic thermal factor refinement using X-PLOR (27) and the

Table 1: X-ray Crystallographic Data Collection Parameters and Refinement Statistics

	Y80F	Q127A	WT "pH 5.5"	WT "pH 4.0"
parameters				
space group	$P2_12_12_1$	$P2_12_12_1$	$P2_12_12_1$	$P2_12_12_1$
cell dimensions (Å)				
<i>a</i>	44.06	43.99	43.87	44.04
<i>b</i>	52.70	52.71	52.78	52.72
<i>c</i>	78.54	78.20	78.36	78.63
no. of measurements	157188	157188	157414	121149
no. of unique reflections	24862	17548	24859	15032
mean $I/\sigma$	28.0 (7.5)	21.8 (6.6)	24.9 (5.4)	30.0 (9.1)
merging $R$ -factor (%) <sup>a</sup>	4.8 (16.2)	5.4 (11.5)	4.8 (21.0)	3.0 (11.0)
resolution range (Å)	∞ to 1.6	∞ to 1.8	∞ to 1.6	∞ to 1.9
refinement statistics				
no. of reflections	24156	15042	23836	13847
resolution range (Å)	10–1.6	10–1.8	10–1.6	10–1.9
completeness within range (%)	95.0	95.0	96.6	93.2
no. of non-hydrogen protein atoms	1447	1444	1448	1448
no. of solvent atoms	196	176	196	129
average thermal factors (Å <sup>2</sup> )				
protein	10.9	9.6	10.4	10.2
solvent	14.1	13.5	13.4	12.9
final refinement $R$ -factor (%)	18.1	16.4	18.5	18.0
stereochemistry, rms deviations				
bonds (Å)	0.006	0.009	0.006	0.007
angles (deg)	1.150	0.911	0.721	1.144

<sup>a</sup> Values in parentheses are for data in the highest resolution shell (1.66–1.60 Å for Y80F BCX, 1.88–1.80 Å for Q127A BCX, 1.66–1.60 Å for WT pH 5.5 BCX, and 1.97–1.90 Å for WT pH 4.0 BCX).

CCP4 Suite (28). At this point  $F_o - F_c$  difference electron density maps were calculated, and the mutated residue was built into observed density with the program O (29). The models were then refined further with X-PLOR, with manual adjustments made periodically during refinement using  $F_o - F_c$ ,  $2F_o - F_c$ , and fragment-deleted difference electron density maps. The validity of solvent molecules was assessed on the basis of both hydrogen-bonding potential to appropriate protein atoms and refinement of a thermal factor of less than 75 Å<sup>2</sup> (Table 1). The rms coordinate errors estimated from Luzzati plots (30) are 0.20 Å for Y80F BCX, 0.18 Å for Q127A BCX, 0.20 Å for WT pH 5.5 BCX, and 0.20 Å for WT pH 4.0 BCX.

Atomic coordinates and related structure factors are deposited in the RCSB Protein Data Bank (31): RCSB PDB ID 1HV0 for Y80F BCX and 1HV1 for Q127A BCX. Structural illustrations using atomic coordinates were generated using the programs Bobscrip (32) and Raster3d (33). Potential hydrogen bonds were identified using the programs HBPLUS (34) and WHAT IF (35), combined with manual inspection of the structures.

**Theoretical  $pK_a$  Calculations.**  $pK_a$  values for the ionizable groups in the WT and mutant forms of BCX were calculated essentially as described previously (36, 37). Briefly, this involved the use of (i) a combination of automated and manual scripts implemented in WHAT IF to construct optimized hydrogen-bonding networks for each ionization state of a given residue, as well as to allow flipping of asparagine, glutamine, and histidine side chains by 180° about their  $\chi_2$ ,  $\chi_3$ , or  $\chi_2$  dihedral angles, respectively (35), (ii) DELPHI to solve the finite-difference Poisson–Boltzmann equation, with uniform dielectric constants of 8 and 80 for the protein and bulk solvent, respectively, an ionic strength of 0.05 M, and a temperature of 25 °C (38), and (iii) a Monte Carlo sampling of the Boltzmann distribution describing the interaction of all ionizable groups in order to

calculate the fractional protonation of each as a function of pH. The  $pK_a$  value of a group is defined as the pH at which it is half-protonated. Pertinent model  $pK_a$  values were Asp (4.0), Glu (4.4), C-terminus (3.8), and His (6.3).

In the cases of WT BCX, as well as N35D, Y69F, Y80F, Q127A, and the covalently modified WT-2FXb and N35D-2FXb variants, the crystallographic coordinates determined at pH 7.5 were utilized directly, without explicit inclusion of bound waters. Generally, the side chains of Asn54, Asn63, Asn114, Gln133, Asn148, and Asn159 (surface residues, distant from the catalytic glutamic acids) were flipped relative to their orientations in the published coordinate files. In the remaining cases of N35A, E78Q, Q127E, R112N, and E172Q BCX, models were constructed by direct amino acid replacements into the WT template. Using WHAT IF to select for the appropriate orientation of the glutamine side chain amides, Gln78 was positioned to hydrogen bond to Tyr69 via its N<sup>ε</sup>H and Q127 via its O<sup>ε2</sup> in E78Q, BCX, and Gln172 positioned to hydrogen bond to Asn35 via its O<sup>ε2</sup> and Tyr80 via its N<sup>ε</sup>H in E172Q BCX.

## RESULTS

**Kinetic Studies.** (i) *Determination of  $k_{cat}$  and  $K_m$  at pH 6.0.* The Michaelis–Menten steady-state kinetic parameters,  $k_{cat}$  and  $K_m$ , were determined at 40 °C and pH 6.0 for the series of BCX mutants using ONPX<sub>2</sub> as a substrate (Figure 2 and Table 2). N35A BCX was the most active mutant with  $k_{cat}/K_m$  values for hydrolysis of ONPX<sub>2</sub> double that exhibited by the WT protein. Although  $k_{cat}$  was reduced by almost 3-fold for this mutant, its overall activity was increased as a result of a greater apparent affinity for the ONPX<sub>2</sub> substrate. A similar, albeit smaller, increase in activity results from the substitution of Asn35 with Asp (3). Other mutants, such as Y80F, R112N, Q127A and Q127E BCX, were still active but showed significantly impaired catalysis relative to the parental WT enzyme. Y80F and R112N BCX had  $k_{cat}/K_m$

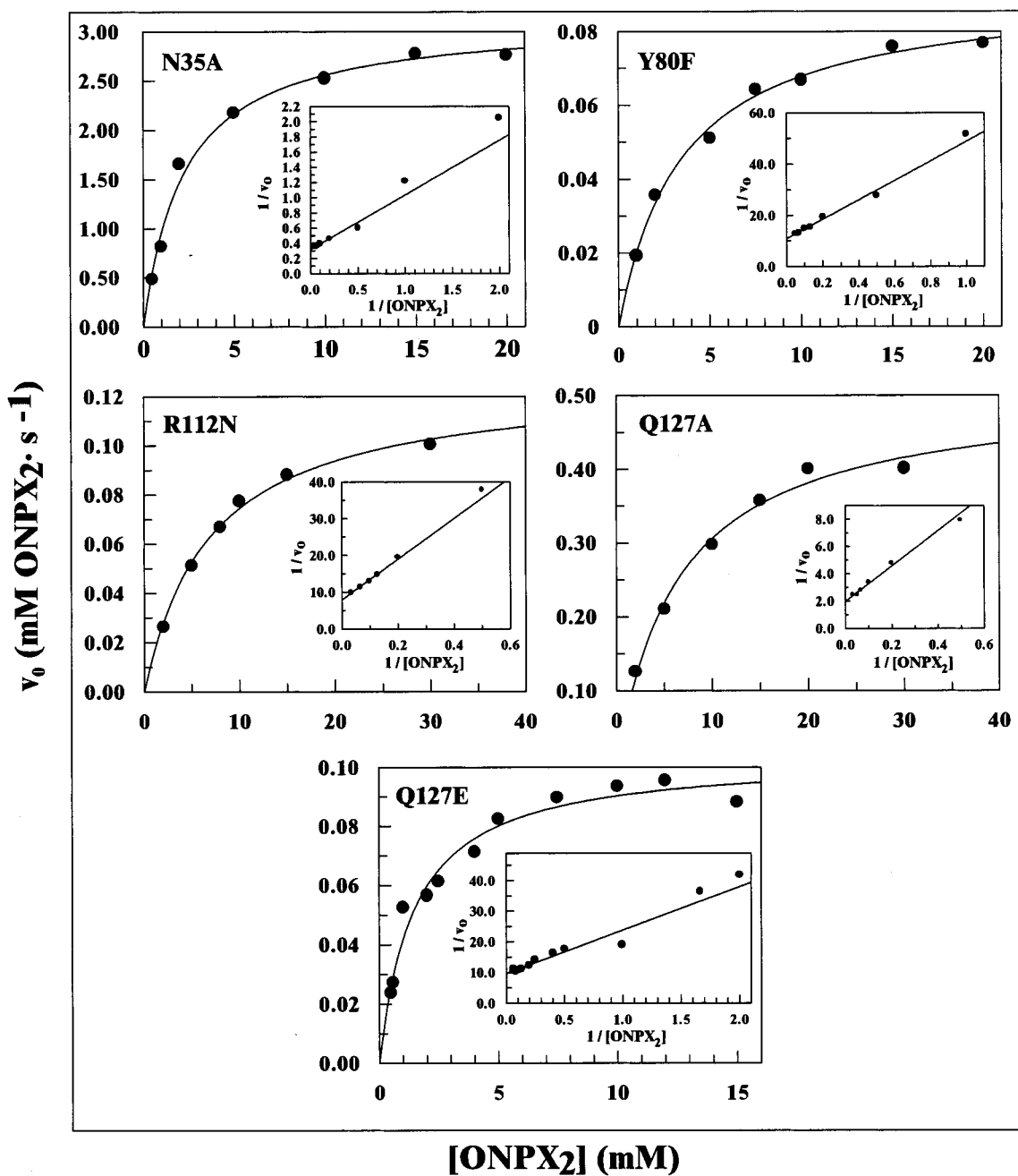


FIGURE 2: Michaelis–Menten plots for BCX mutant proteins at 40 °C and pH 6.0 reveal that each enzyme exhibits saturation kinetics toward the synthetic substrate ONPX<sub>2</sub>. Furthermore, Lineweaver–Burk plots (inserted) are linear, indicating a lack of significant transglycosylation activity at elevated substrate concentrations. For each mutant,  $k_{cat}$  and  $K_m$  were extracted by nonlinear least-squares fitting of the initial rates,  $v_0$ , to a standard Michaelis–Menten expression, whereas the value of  $k_{cat}/K_m$  was determined from the slope of the Lineweaver–Burk plot. These kinetic parameters are summarized in Table 2.

values that were reduced by >95% compared to WT BCX, mainly due to decreases in  $k_{cat}$  by approximately 2 orders of magnitude. Substitutions at position 127 with an Ala (Q127A) and a Glu (Q127E) led to similar reductions in  $k_{cat}/K_m$  to about 10% of that of WT BCX. The parameter  $k_{cat}$  was reduced to a greater extent in Q127E, yet this was compensated by a favorable change in  $K_m$ , yielding an overall activity comparable to Q127A. On the far end of the spectrum of mutants was Y69F BCX, with the substitution of a Phe for Tyr69 resulting in virtual abolition of activity. Thus, with one exception, the overall activities (based on values of  $k_{cat}/K_m$ ) of the xylanases with active site mutations were reduced significantly when compared to WT BCX,

primarily due to reductions in their  $k_{cat}$  values.

For comparison, Table 2 also summarizes kinetic data published previously for variants of BCX with substitutions at positions 35, 78, and 172 (3–6). As expected, mutation of the nucleophile Glu78 to glutamine or cysteine abolishes the activity of BCX, while substitution with aspartic acid allows a very small degree of hydrolysis to occur. In the case of activated substrates, such as ONPX<sub>2</sub>, general acid catalysis is not absolutely required (39); thus the same substitutions at position 172 have less dramatic effects.

(ii) *pH Dependence of Activity.* To further characterize the mutant xylanases, their  $k_{cat}/K_m$  values for the hydrolysis of ONPX<sub>2</sub> were measured as a function of pH at 40 °C. There

Table 2: Steady-State Kinetic Parameters for the Hydrolysis of ONPX<sub>2</sub> by WT and Mutant BCX Proteins<sup>a</sup>

protein	$k_{\text{cat}}^b$ (s <sup>-1</sup> )	$K_m^b$ (mM <sup>-1</sup> )	$k_{\text{cat}}/K_m^b$ (s <sup>-1</sup> mM <sup>-1</sup> )	activity <sup>c</sup> (% of WT)	pK <sub>a</sub> Glu78 <sup>d</sup>	pK <sub>a</sub> Glu172 <sup>d</sup>	pH <sub>optimum</sub> <sup>e</sup>
WT <sup>f</sup>	9.58	14.2	0.70	100 (103)	4.6 (4.6)	6.8 (6.7)	5.7
N35A	3.13	2.2	1.40	200 (207)	4.4 (4.5)	6.9 (6.9)	5.7
Y69F <sup>g</sup>					— (4.9)	— (8.3)	
Y80F	0.09	3.5	0.03	4 (4)	4.8 (5.0)	7.7 (7.9)	6.3
R112N	0.13	7.0	0.02	3 (3)	4.5 (5.0)	7.8 (7.6)	6.2
Q127A	0.51	6.7	0.08	11 (11)	4.1 (4.2)	7.3 (7.3)	5.7
Q127E	0.10	1.5	0.07	10 (12)	3.6 (3.8)	6.5 (6.5)	5.1
N35D <sup>h</sup>	14.5	25.6	0.56	85 (190)	3.5 (5.7) <sup>i</sup>	5.8 (8.4) <sup>i</sup>	4.6
N35D/E172Q <sup>h</sup>	0.72	33.3	0.021	4	<i>j</i>	<i>j</i>	<i>j</i>
N35D/E78Q <sup>g,h</sup>							
E172Q <sup>f</sup>	0.62	8.3	0.075	11	(5.1) <sup>j</sup>		<i>j</i>
E172C <sup>f</sup>	0.40	2.5	0.16	23	4.0 <sup>j</sup>	<i>j,k</i>	<i>k</i>
E172D <sup>f</sup>	0.25	7.2	0.03	4	4.2	8.0	6.1
E78Q <sup>f</sup>						(4.2) <sup>j</sup>	
E78C <sup>f</sup>							
E78D <sup>f</sup>	0.005	14.0	0.0004				

<sup>a</sup> Assays were carried out at pH 6.0 and 40 °C. <sup>b</sup> Values of  $k_{\text{cat}}/K_m$  were taken from the slope of the Lineweaver–Burk plot, whereas values of  $k_{\text{cat}}$  and  $K_m$  were determined from a nonlinear fit of the Michaelis–Menten equation. The differences between the measured  $k_{\text{cat}}/K_m$  and those calculated from the latter two parameters are small, reflecting the precision of the data fitting and the lack of significant transglycosylation activity at elevated substrate concentrations (Figure 2). <sup>c</sup> Based on relative  $k_{\text{cat}}/K_m$  values determined at pH 6.0 and 40 °C. Values in parentheses are the ratios of the values of  $k_{\text{cat}}/K_m$  interpolated to the pH optimum of each enzyme. <sup>d</sup> Apparent pK<sub>a</sub> values were determined by fitting the data to the bell-shaped activity profiles shown in Figure 3. Errors in these pK<sub>a</sub> values, determined from data fitting, are less than or equal to the error of pH measurement of ±0.1 units. With the exception of N35D BCX, the pK<sub>a</sub> of the acidic limb is attributed to Glu78 and that of the basic limb to Glu172. Corresponding macroscopic pK<sub>a</sub> values measured by NMR, and listed in Table 3, are indicated in parentheses. <sup>e</sup> pH<sub>optimum</sub> = (pK<sub>a</sub>Glu78 + pK<sub>a</sub>Glu172)/2. <sup>f</sup> Data were taken from Lawson et al. (4) and/or McIntosh et al. (6). <sup>g</sup> No detectable enzymatic hydrolysis. <sup>h</sup> Data were taken from Joshi et al. (3). <sup>i</sup> N35D BCX follows a reverse protonation mechanism. See Joshi et al. (3) for an extensive discussion. <sup>j</sup> NMR and/or kinetic data are unavailable. <sup>k</sup> The pH-dependent activity profile showed that the basic limb was invariant up to the limit of the assay conditions (pH 9), and hence the pK<sub>a</sub> of Cys172 was undeterminable. <sup>l</sup> Data were taken from Lawson et al. (4).

are several advantages to monitoring this kinetic parameter rather than  $k_{\text{cat}}$  or  $K_m$  alone. First, since  $k_{\text{cat}}/K_m$  is the second-order rate constant for the reaction of free enzyme and substrate, we are able to interpret its pH dependence in terms of ionization events related specifically to the unbound enzyme. This allows for a direct comparison of the apparent pK<sub>a</sub> values, extracted from bell-shaped  $k_{\text{cat}}/K_m$  versus pH activity profiles, with those measured site-specifically for Glu78 and Glu172 by <sup>13</sup>C NMR. The use of  $k_{\text{cat}}$  would not have allowed for this comparison, as this first-order rate constant reflects bound species including the enzyme–substrate, –intermediate, and –product complexes. Parenthetically, however, previous studies have shown that the  $k_{\text{cat}}$  and  $k_{\text{cat}}/K_m$  values of the WT enzyme toward this neutral substrate have similar pH dependencies due to  $K_m$  being essentially constant (6). Second, since  $k_{\text{cat}}/K_m$  always reflects the events up to and including the first *irreversible* step in the mechanism (in this case the initial C–O bond cleavage), its value will not be influenced by potential changes in the rate-determining step (e.g., from glycosylation to deglycosylation) that may result from active site mutation. Third, and perhaps experimentally most important, it is also difficult to interpret  $K_m$  and  $k_{\text{cat}}$  values individually when competing transglycosylation reactions can potentially occur at elevated substrate concentrations. In contrast, the ratio of these kinetic constants, given by  $k_{\text{cat}}/K_m$ , may be accurately measured and interpreted from a pseudo-first-order analysis of the reaction velocity under conditions of limited substrate.

Data summarizing the pH dependence of  $k_{\text{cat}}/K_m$  for the hydrolysis of ONPX<sub>2</sub> by the mutant xylanases with measurable activity are presented in Table 2 and Figure 3. As readily seen in this figure, each of these enzymes exhibited a classical bell-shaped activity versus pH profile. Previous studies of WT BCX have shown that deprotonation of the

nucleophile, Glu78 (pK<sub>a</sub> 4.6), leads to the increase in activity on the acidic limb of this curve, while ionization of the general acid catalyst, Glu172 (pK<sub>a</sub> 6.7), causes the loss in activity on the basic limb (6, 8, 16). As confirmed below using NMR methods, this assignment of kinetically determined apparent pK<sub>a</sub> values to the two catalytic residues remains valid for each BCX mutant studied herein. Replacement of an Ala for Asn in N35A BCX resulted in minimal changes in the pK<sub>a</sub> values controlling both limbs of its activity profile (pK<sub>a</sub>Glu78 = 4.4, pK<sub>a</sub>Glu172 = 6.9). Thus, while the overall activity of N35A was doubled relative to WT BCX, its pH optimum remained unchanged at 5.7. The activity profile of Y80F BCX followed apparent pK<sub>a</sub> values of 4.8 and 7.7 for the acidic and basic limbs, respectively. This resulted in a change in pH optimum of Y80F from 5.7 to 6.3, due mainly to the increase in the apparent pK<sub>a</sub> value of Glu172 by ~1 unit. Similarly, the pH optimum of R112N BCX shifted from 5.7 in the WT to a more basic value of 6.2. This was also due mainly to an elevation of the apparent pK<sub>a</sub> value of Glu172 from 6.7 to 7.8.

The two substitutions at position 127, Q127A and Q127E, resulted in similar reductions in  $k_{\text{cat}}/K_m$  relative to WT BCX but different pH-dependent activity profiles. The profile of Q127A followed apparent pK<sub>a</sub> values of 4.1 and 7.3 for the acidic and basic limbs, respectively. Thus, while its pH optimum did not change relative to WT BCX, its activity profile was broadened. The Q127E BCX mutant was different from the other mutants discussed so far in that it was a substitution where a potentially negatively charged residue was introduced into the active site. This resulted in a shift of the pH optimum of Q127E from 5.7 to a more acidic value of 5.1. Most notable was the decrease in the apparent pK<sub>a</sub> value of the acidic limb, corresponding to the

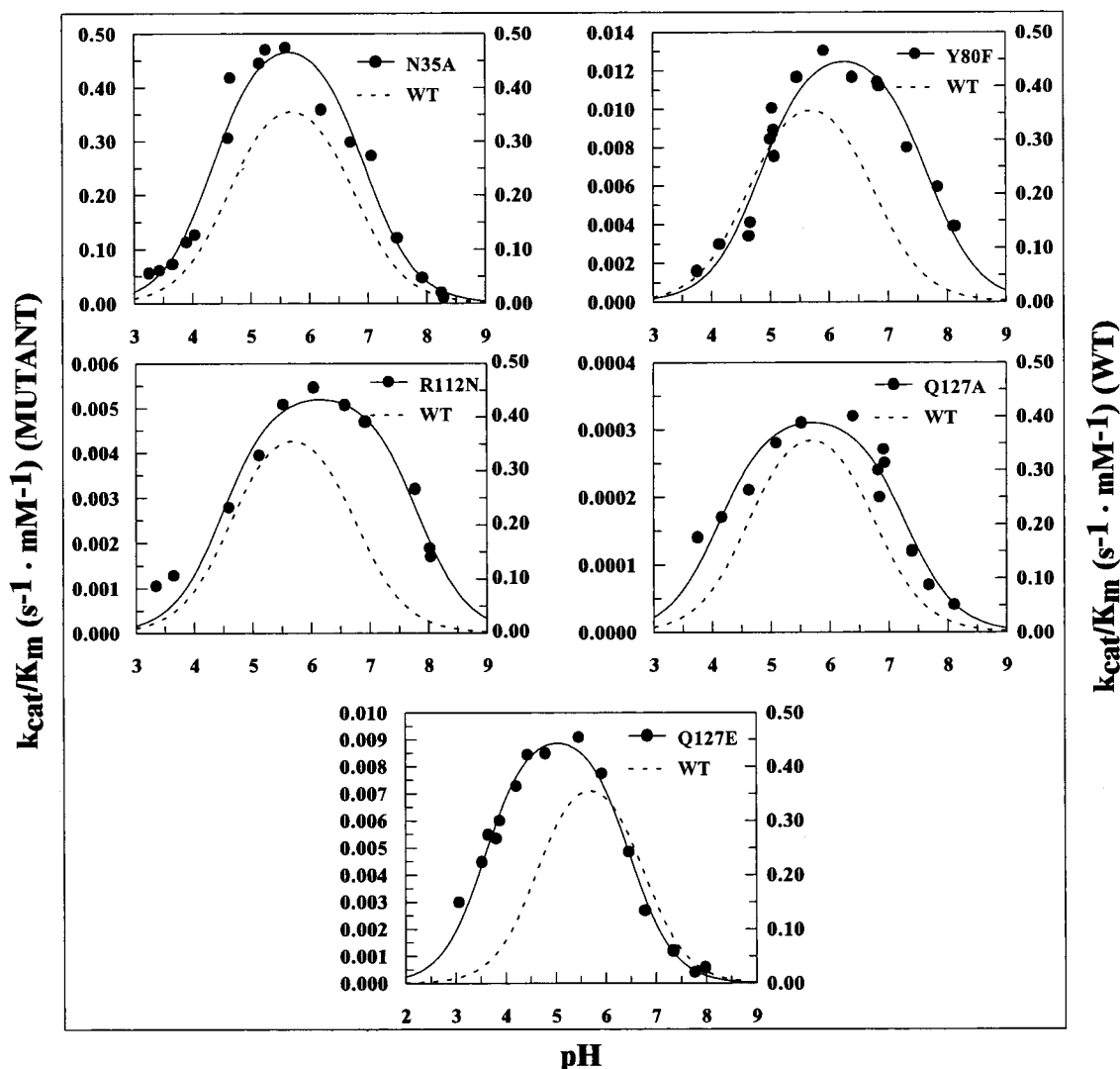


FIGURE 3: pH dependence of  $k_{cat}/K_m$  for BCX mutant proteins (●) at 25 °C toward the substrate ONPX<sub>2</sub>. As confirmed by NMR spectroscopic studies, the acidic and basic limbs of the activity profiles follow the ionizations of Glu78 and Glu172, respectively. The pH optima of N35A and Q127A BCX remained unchanged at the WT value of 5.7 with an approximate doubling of relative activity of N35A BCX compared to WT. Y80F and R112N BCX functioned optimally under slightly more basic conditions with pH optima of 6.3 and 6.2, respectively, while Q127E BCX showed optimal activity under more acidic conditions and had an optimum of 5.1. The data points, shown only for the mutant BCX proteins, were fitted (solid line) as described in Experimental Procedures, and apparent  $pK_a$  values are listed in Table 2. The fitted profile for the WT enzyme (dashed lines) is characterized by a pH optimum of 5.7 and follows  $pK_a$  values of 4.6 and 6.7 (6). Note the different ordinate scales for the WT (right) and mutant enzymes (left).

ionization of Glu78, by 1 pH unit from 4.6 to 3.6, combined with a smaller decrease of 0.3 units for the basic limb (Glu172). Other studies have shown that the substitution of Asn35 by a negatively charged Asp also shifts the pH optimum of BCX to a more acidic value of 4.6 (3).

In summary, the active site substitutions altered the pH-activity profile of BCX, in terms of both pH optima and/or the apparent  $pK_a$  values of the acidic and basic limbs. In particular, the mutations Y80F and R112N led to a small elevation in the pH optimum, due primarily to an increase in the  $pK_a$  assignable to Glu172. The reverse trend occurred with Q127E, with the  $pK_a$  of Glu78 being most influenced. Since the pH optima of the mutant enzymes are shifted relative to WT BCX, Table 2 also provides a comparison of their maximum  $k_{cat}/K_m$  values at 40 °C. These relative activities were comparable to those discussed previously for measurements made at a fixed pH of 6.0 and indicated that, with the exception of N35A and N35D, mutation of active

site residues generally impaired the catalytic ability of BCX under all pH conditions.

(iii) *Pre-Steady-State Kinetics*. Each of the xylanases was analyzed by rapid stopped-flow methods to determine if the rate-determining step had changed from glycosylation to deglycosylation as a result of mutation. Using ONPX<sub>2</sub> as a substrate, none of the proteins analyzed showed the presence of a diagnostic pre-steady-state burst phase (data not shown). Hence, it appears that glycosylation is the rate-limiting step for WT BCX and all mutants examined toward ONPX<sub>2</sub> and that the values listed for  $k_{cat}$  in Table 2 correspond to the  $k_2$  rate constant in Scheme 1.

In addition to ONPX<sub>2</sub>, the substrate 2,5-DNPX<sub>2</sub> was tested because its better leaving group ( $pK_a$  7.22 versus 5.15, respectively) (39) would allow deglycosylation, if rate-limiting, to become more dominant and thus kinetically visible (24). In the case of Y80F BCX, stopped-flow kinetic studies clearly indicated a pre-steady-state burst with this

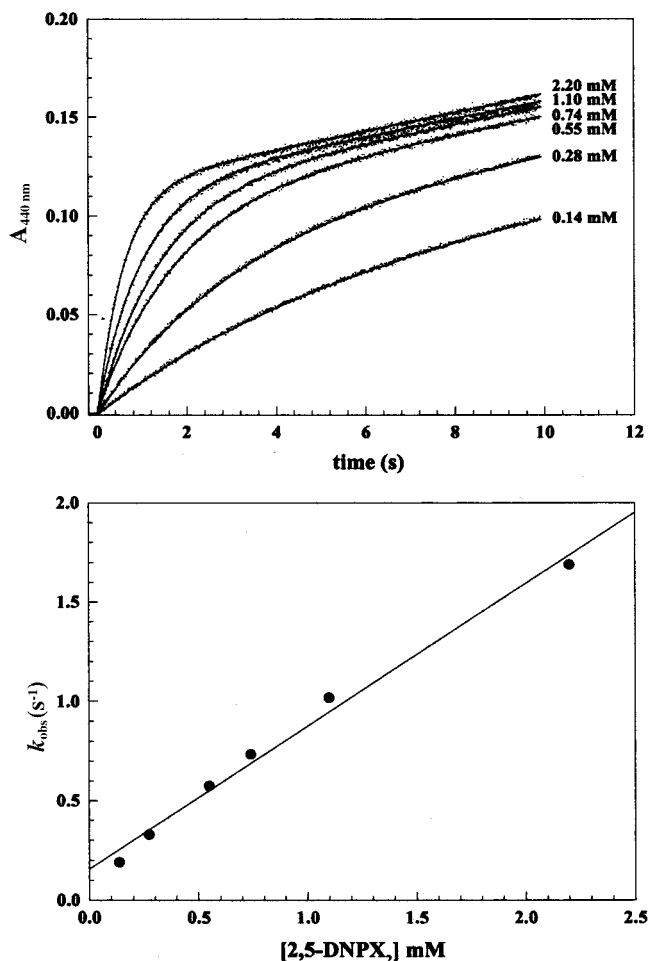


FIGURE 4: Pre-steady-state kinetic analysis of the hydrolysis of 2,5-DNPX<sub>2</sub> by Y80F BCX at 25 °C and pH 6.0 monitored by stopped-flow UV-vis spectroscopy. This system showed an initial exponential pre-steady-state burst phase, indicating the accumulation of a glycosyl-enzyme intermediate, followed by a linear steady-state phase due to its subsequent turnover (upper plot). First-order rate constants for the exponential pre-steady-state phase ( $k_{\text{obs}}$ ) were determined at each substrate concentration by fitting the experimental data in the upper plot, indicated by small circles, to an expression with an exponential and linear term (—). Values of  $k_{\text{obs}}$  (●) were then plotted as a function of 2,5-DNPX<sub>2</sub> concentration in order to determine the second-order rate constant  $k_2/K_d$  of 0.72 mM<sup>-1</sup> s<sup>-1</sup> (lower plot).

readily hydrolyzable substrate (Figure 4). Thus with this system,  $k_2$  (glycosylation) >  $k_3$  (deglycosylation), and the formation and accumulation of the glycosyl-enzyme intermediate are kinetically observable. This result is consistent with the low  $K_m$  value (0.060 mM) (22) observed for this substrate compared to WT (2.2 mM) (5). Fitting of the first-order rate constants ( $k_{\text{obs}}$ ) determined at each substrate concentration to eq 8 yielded a value of  $k_2/K_d$  of 0.72 mM<sup>-1</sup> s<sup>-1</sup>. This closely matches the previously measured value of 0.70 mM<sup>-1</sup> s<sup>-1</sup> for the corresponding second-order rate constant  $k_{\text{cat}}/K_m$  of Y80F BCX reacting with 2,5-DNPX<sub>2</sub> (22), indicating a rapid binding equilibrium before catalysis ( $k_{-1}$  >  $k_2$  in Scheme 1). The results obtained for Y80F were therefore in excellent overall agreement with those obtained previously by Zechel et al. (22) in their founding study of the use of time-resolved electrospray ionization mass spectrometry for the accurate determination of pre-steady-state kinetic parameters.

*Direct Measurement of the pK<sub>a</sub> Values of Glu78 and Glu172 by <sup>13</sup>C NMR.* To correlate the pH-activity profiles with the ionizations of the catalytic residues, <sup>13</sup>C NMR was utilized to measure directly the pK<sub>a</sub> values of Glu78 and Glu172 in each of the mutant proteins. Specifically, the carbonyl <sup>13</sup>C chemical shifts of the Glu and Gln side chains were monitored in selectively isotopically labeled proteins over the course of a pH titration (Figure 5). The assignment of these resonances were based upon previous studies of WT BCX (6) and were confirmed by the notable exchange broadening of the resonance of Glu172 centered at its pK<sub>a</sub> value. As seen previously for WT BCX, the titration curves of Glu78 and Glu172 were multiphasic in the case of each mutant xylanase (6). Note that two or more ionizable groups may show coupled or biphasic titration curves if either the microscopic pK<sub>a</sub> or the chemical shift of one is dependent upon the ionization state of the other (25; M. D. Joshi, J. E. Nielsen, and L. P. McIntosh, in preparation). The first case is analogous to the classic example of a dibasic acid in which each carboxyl has two microscopic pK<sub>a</sub> values corresponding to the neutral and charged states of its interacting partner. The second case reflects the possibility that the chemical shift of one residue can be sensitive to the ionization state of another, for example, through electric field effects or structural perturbations. As previously (3, 6), we fitted the titration curves measured for each mutant to simple equations describing sequential ionization equilibria in order to extract apparent or macroscopic pK<sub>a</sub> values. The apparent pK<sub>a</sub> value that corresponded to the largest positive chemical shift change (ionized versus neutral) of each Glu residue was attributed to reflect its own ionization, while those that contributed to smaller chemical shift changes were assigned to the ionization equilibria of neighboring residues. In parallel, these titration data were also analyzed according to a model of microscopic pK<sub>a</sub> values (Scheme 2 and Figure S1, Supporting Information).

The pH titration of N35A BCX showed that both Glu78 and Glu172 exhibited biphasic titration behavior (Figure 5 and Table 3). Two macroscopic pK<sub>a</sub> values were observed for Glu78. The first, with a major chemical shift change of +3.09 ppm, followed a pK<sub>a</sub> value of 4.5 and was assigned to the ionization of Glu78 itself. The second, with a minor chemical shift change of +0.12 ppm, followed a pK<sub>a</sub> value of 6.8 and reflected the ionization of Glu172. Similarly, the titration curve of Glu172 followed two macroscopic pK<sub>a</sub> values. The first, with a minor chemical shift change of +0.44 ppm, followed a pK<sub>a</sub> value of 4.9 and thus reflected the ionization of Glu78. The second, with a major chemical shift change of +2.81 ppm at a pK<sub>a</sub> value of 6.9, represented the ionization of Glu172 itself. The pH-dependent spectra of other mutants (Y69F, Y80F, Q127A, and R112N BCX) were assigned and analyzed in a manner similar to that of N35A. In each case, the titration curves for Glu78 and Glu172 were consistently biphasic. Although the magnitudes of the spectral changes varied between mutants, a major positive chemical shift could always be identified as reflecting the protonation equilibrium of the glutamate whose resonance was being followed. Thus, the mutation of Tyr80 to Phe (Y80F BCX) yielded predominant pK<sub>a</sub> values of 5.0 for Glu78 and 7.9 for Glu172. In R112N BCX, Glu78 and Glu172 titrated with pK<sub>a</sub> values of 5.0 and 7.6, respectively. The titration of Q127A BCX yielded a pK<sub>a</sub> value of 4.2 for

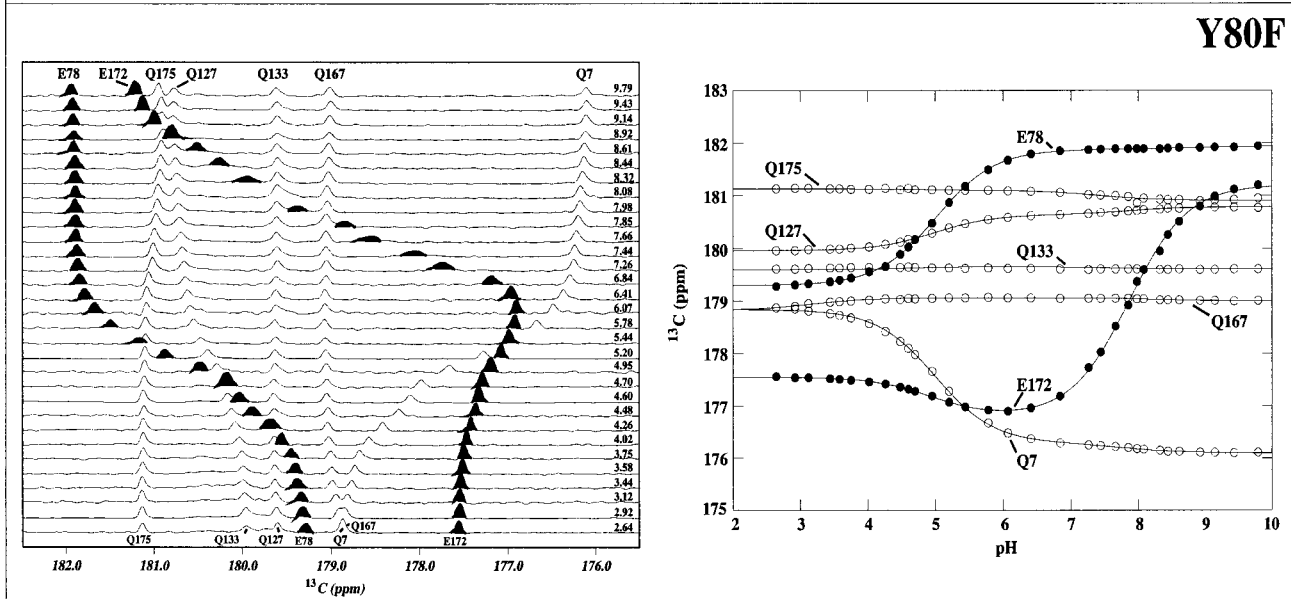
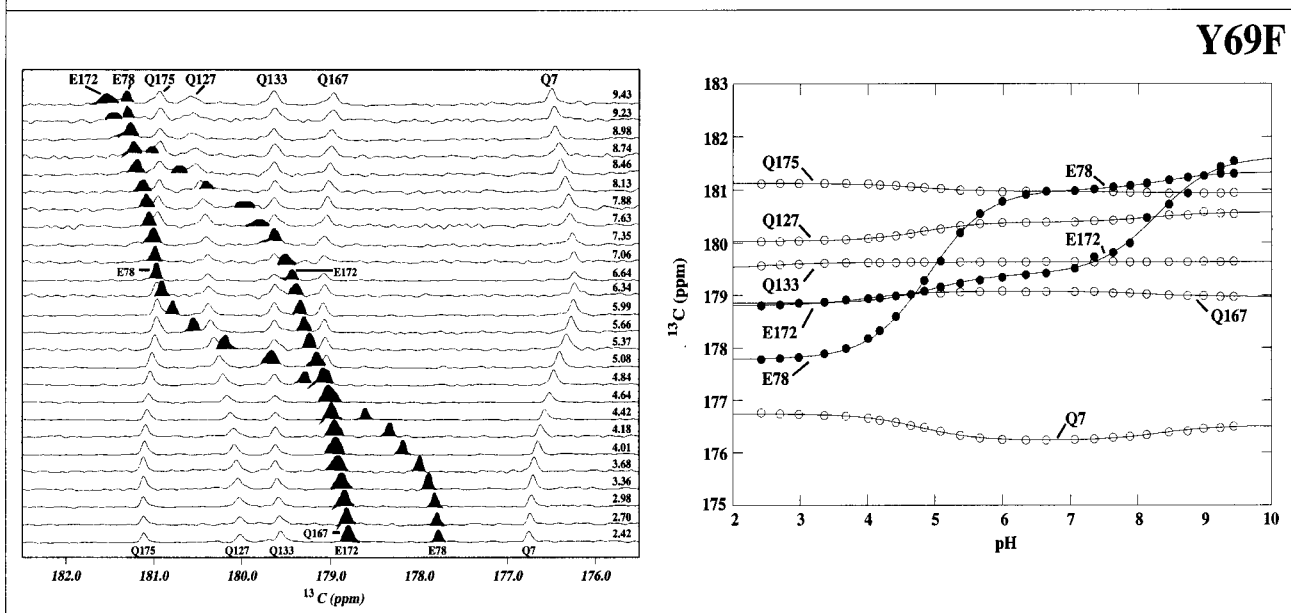
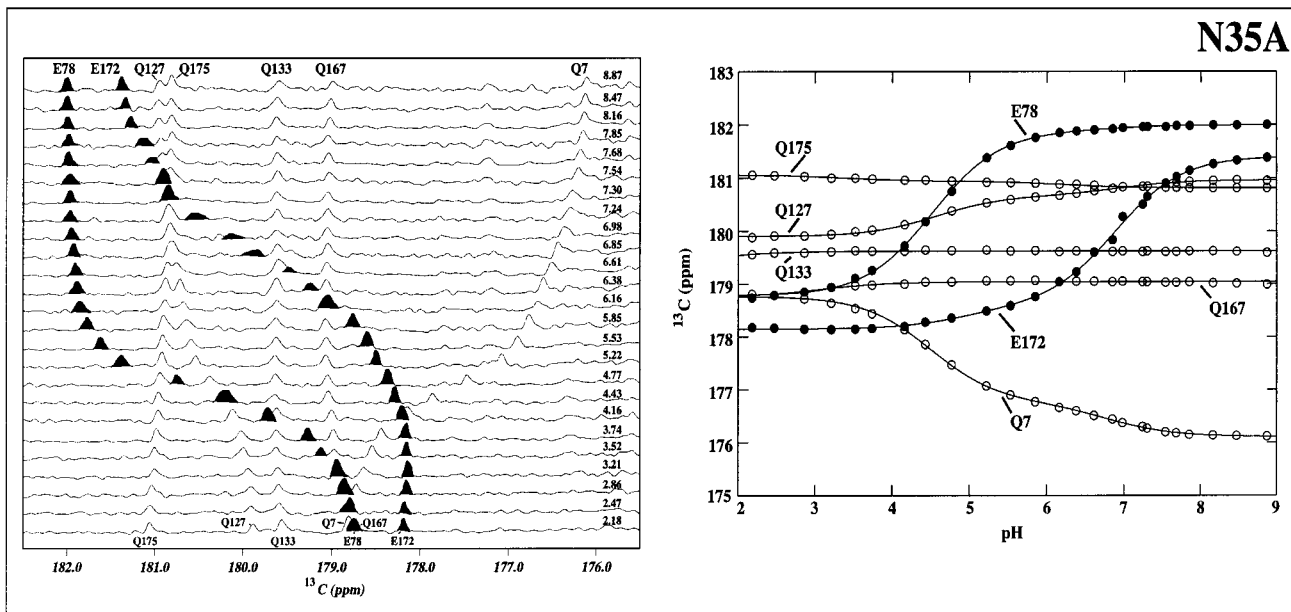




FIGURE 5:  $^{13}\text{C}$  NMR spectra of mutant BCX proteins recorded as a function of pH at 25 °C. The peaks corresponding to Glu78, Glu172, and, in the case of Q127E BCX, Glu127 are shaded in black or gray, respectively, for emphasis. Spectral assignments are based on a previous analysis of WT BCX (6), and pH values are listed above each spectrum (right-hand side). Apparent  $pK_a$  values were determined by fitting the data for the two catalytic Glu (●) and five Gln (○) carbonyl groups to an equation describing the pH dependence of the chemical shift of a residue to one or more sequential ionization events. Data used for the fitting of Glu127 in Q127E BCX are also indicated by an open circle (○) symbol.

Table 3: Experimentally Measured Apparent  $pK_a$  Values of WT and Mutant BCX Proteins Obtained from  $^{13}\text{C}$  NMR pH Titrations<sup>a</sup>

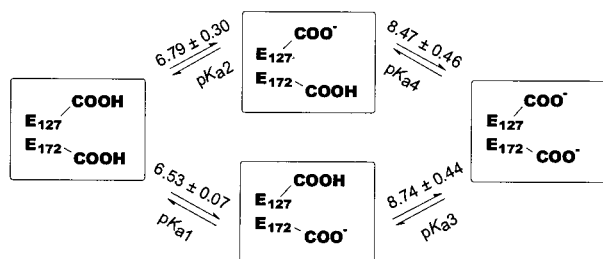
protein	$\delta\Delta$ (ppm) <sup>c</sup>		$\delta\Delta$ (ppm) <sup>c</sup>		$\Delta pK_{a\text{Glu78}}^d$	$\Delta pK_{a\text{Glu172}}^d$
	$pK_{a\text{Glu78}}$		$pK_{a\text{Glu172}}$			
WT <sup>b</sup>	<b>4.6</b>	+2.80	4.6	+0.44	0	0
	6.5	+0.33	<b>6.7</b>	+2.78		
N35A	<b>4.5</b>	+3.09	4.9	+0.44	-0.1	
	6.8	+0.12	<b>6.9</b>	+2.81		
Y69F	<b>4.9</b>	+3.21	5.0	+0.55	+0.3	
	8.9	+0.33	<b>8.3</b>	+2.22		
Y80F	<b>5.0</b>	+2.58	4.9	-0.75	+0.4	
	8.8	+0.06	<b>7.9</b>	+4.40		
R112N	<b>5.0</b>	+3.96	4.8	-0.16	+0.4	
	7.5	-0.71	<b>7.6</b>	+3.67		
Q127A	<b>4.2</b>	+3.52	4.5	+0.42	-0.4	
	7.6	-0.06	<b>7.3</b>	+3.03		
Q127E <sup>e</sup>	<b>3.8</b>	+2.88	3.8	-0.25	-0.8	
	6.6	+0.34	<b>6.5</b> <sup>f</sup>	+3.08		
	8.6 <sup>g</sup>	+0.21	9.0	+1.74		
N35D <sup>h</sup>	4.2	+0.96	4.0	+0.76		
	<b>5.7</b>	+2.69	5.5	-0.32		
	8.4	-0.39	<b>8.4</b>	+3.09		
N35D-2FXb <sup>h</sup>	2.9 <sup>j</sup>	-0.03	<b>1.9</b> <sup>i</sup>	+1.63	<i>j</i>	
	9.3 <sup>j</sup>	-0.18	<b>3.4</b> <sup>i</sup>	+0.48		
			9.0	+0.10		
WT-2FXb	<i>k</i>	<i>k</i>	<b>4.2</b>	+1.58	<i>k</i>	-2.5
E172Q <sup>b,l</sup>	<b>5.1</b>	+3.93	5.1 <sup>j</sup>	-0.48 <sup>j</sup>	+0.5	<i>i</i>
E78Q <sup>b,l</sup>	<i>k</i>	<i>k</i>	<b>4.2</b>	+3.81	<i>k</i>	-2.5

<sup>a</sup> The major apparent  $pK_a$  assigned to the ionization of the given residue is boldfaced. An error in the  $pK_a$  value of  $\pm 0.1$  pH unit is estimated from the error in pH measurements. <sup>b</sup> Data were taken from McIntosh et al. (6). <sup>c</sup> The  $\delta\Delta$  value refers to the magnitude and direction of the chemical shift change upon deprotonation of the listed residue. The error in chemical shift is estimated to be  $\pm 0.015$  ppm. <sup>d</sup>  $\Delta pK_a = pK_a(\text{mutant}) - pK_a(\text{WT})$  (differences are calculated using the major  $pK_a$  values of the mutant and WT). <sup>e</sup> Data for Glu127 were fitted to give  $pK_a$  values of 3.7 ( $\delta\Delta = +0.74$  ppm), 6.4 ( $\delta\Delta = +1.10$  ppm), and 8.4 ( $\delta\Delta = +1.52$  ppm). <sup>f</sup> The assignment of the major  $pK_a$  for Glu172 in Q127E BCX is tentative. Simultaneous fitting of the titration curves measured for Glu172 and Glu127 yields microscopic  $pK_a$  values of 6.5 and 8.5 for Glu172 and 6.8 and 8.7 for Glu127 (corresponding to ionization in the presence of a neutral or charged partner; see Scheme 2). <sup>g</sup> The third and minor  $pK_a$  value of 8.6 for Glu78 was determined from fitting the data from pH 5–10 only. <sup>h</sup> Data were taken from ref 3. Asp35 yielded  $pK_a$  values of 3.7 ( $\delta\Delta = +2.13$  ppm), assigned to its titration, and 5.6 ( $\delta\Delta = +1.07$  ppm), attributed to the ionization of Glu78. <sup>i</sup> Glu172 and Asp35 are assigned to titrate as a coupled pair, with the first  $pK_a \sim 1.9$ –3.4 and the second  $pK_a > 9$ .  $\Delta pK_{a\text{Glu172}}$  is relative to the unmodified N35D BCX (3). <sup>j</sup> Change in chemical shift does not reflect ionization of the residue itself since it has either been substituted with a residue with a nonionizable side chain or has been modified by covalent attachment to the inhibitor. <sup>k</sup> No observable pH-dependent change in chemical shift. <sup>l</sup> E78Q and E172Q are in the background of *B. subtilis* xylanase, which differs from BCX by the nonperturbing substitution of T147S on the surface of the protein (6).

Glu78 and a  $pK_a$  value of 7.3 for Glu172. Finally, although the  $pK_a$  values of Y69F BCX could not be determined from kinetic pH–rate profiles due to the inactivity of the protein, they were readily measured to be 4.9 (Glu78) and 8.3 (Glu172) by  $^{13}\text{C}$  NMR methods. Interestingly, with Y80F and R112N BCX, minor chemical shift changes due to the protonation of the adjacent glutamate were negative in sign, illustrating the potential complexity in interpreting pH-dependent spectral changes in proteins.

The titration behavior of Q127E BCX was markedly different than the other variants analyzed due to the presence of an additional Glu residue in the active site. Note that this new Glu replaces Glu127, which is directly hydrogen bonded to Glu78 in WT BCX. The resonance assignment of Glu78 was straightforward, based on its chemical shift at neutral pH and its titration behavior. Although the resonance assignments of Glu172 and Glu127 were difficult to make from chemical shift and titration behavior alone, the exchange broadening observed in all BCX variants for Glu172 was used to distinguish the signals from these two glutamic acids (6). The titration curve of Glu78 was triphasic and followed three macroscopic  $pK_a$  values. The first, with a major change in chemical shift change of +2.88 ppm, fitted to a  $pK_a$  value of 3.8 and was assigned to the ionization of Glu78 itself. The second and third, with minor changes in chemical shift of +0.34 and +0.21 ppm, followed  $pK_a$  values of 6.6 and 8.6, respectively, and are attributed to the ionizations of the remaining two glutamic acids. The titration curve of Glu172 was triphasic in nature and reflected three ionizations. The first, corresponding to a minor change in chemical shift of -0.25 ppm, followed a  $pK_a$  value of 3.8 and likely reflected the ionization of Glu78. The second, corresponding to the largest change in chemical shift of +3.08 ppm, followed a  $pK_a$  of 6.5 and was assigned primarily to the ionization of Glu172 itself. The third, corresponding to a change in chemical shift of +1.74 ppm, followed a  $pK_a$  value of 9.0 and was attributed to Glu127. These tentative assignments are supported by the pH–activity profile of Q127E BCX, which showed apparent  $pK_a$  values of 3.6 and 6.5 that, by inference to all other mutants studied herein, can be attributed to Glu78 and Glu172, respectively. The titration curve of Glu127 in Q127E BCX was also triphasic and followed three macroscopic  $pK_a$  values. The first  $pK_a$  value of 3.7, accompanied by a minor change in chemical shift of +0.74 ppm, likely corresponded to the ionization of Glu78. The second  $pK_a$  value of 6.4 was accompanied by a chemical shift change of +1.10 ppm and was assigned to an indirect perturbation due to Glu172. Finally, the third  $pK_a$  value of 8.4, accompanied by the largest change in chemical shift of +1.52 ppm, likely corresponded to the ionization of Glu127 itself. The  $pK_a$  value for Glu127 of either 9.0, from the titration curve of Glu172, or the  $pK_a$  value of 8.4, from the titration curve of Glu127, may be underestimated since no distinct titration plateau or base line was observed in the basic pH range of the titration. Note that we could not unambiguously assign the  $pK_a$  values of Glu127 and Glu172 from these NMR data as both showed titrations near pH 6.5 and  $> 8$  with pronounced chemical shift changes. Thus, instead of fitting these data to eq 11, which yields macroscopic or averaged  $pK_a$  values, the titrations can also be analyzed in terms of microscopic  $pK_a$  values (3, 6; M. D. Joshi, J. E. Nielsen, and L. P. McIntosh, in preparation). Simultaneous fitting of the titration data, for these two residues, in the pH range from 6 to 11 (i.e., with Glu78 deprotonated) yields Scheme 2.

Scheme 2



By this analysis, Glu172 ionizes with a  $pK_a$  of 6.5 or 8.5 in the presence of a neutral or charged Gln, respectively. Similarly, Glu127 exhibits a  $pK_a$  value of 6.8 or 8.7 in the presence of the carboxylic acid or carboxylate forms of Glu172. The ionization pathway favors the lower limb of this scheme, with microscopic  $pK_a$  values corresponding to the macroscopic values discussed above.

The  $^{13}\text{C}$  NMR resonances of the side chain  $\delta$  carbonyls of all Gln residues were also detected in the  $^{13}\text{C}$  NMR spectra of all of the proteins analyzed. Their presence is due to the metabolic interconversion of glutamic acid to glutamine in *E. coli*. The  $^{13}\text{C}$  chemical shifts of the nonionizable Gln residues are pH-dependent because of the influence of other titratable side chains within the protein. Thus these served as reporter groups to further verify the  $pK_a$  values measured for the glutamic acid residues. For example, in Q127E BCX the pH-dependent chemical shift of Gln7 followed three  $pK_a$  values, namely, 3.51 ( $\delta\Delta = 0.67$  ppm), 6.40 ( $\delta\Delta = 1.06$  ppm), and 9.04 ( $\delta\Delta = 0.27$  ppm). These were assigned to reflect the ionizations of Glu78, Glu172, and Glu127, respectively. Similarly, in R112N BCX, the pH-dependent chemical shift of Gln7 predominantly followed two  $pK_a$  values, namely, a  $pK_a$  of 4.9 ( $\delta\Delta = 1.90$  ppm) due to the ionization of Glu78 and a  $pK_a$  of 7.4 ( $\delta\Delta = 0.20$  ppm) due to the ionization of Glu172. In the WT protein, the resonance of Gln7 followed the titrations of Glu78 ( $pK_a$  4.5,  $\delta\Delta = 2.09$  ppm) and Glu172 ( $pK_a$  6.6,  $\delta\Delta = 0.47$  ppm) (6).

In general, the  $pK_a$  values of Glu78 and Glu172 determined from the pH dependence of  $k_{\text{cat}}/K_m$  are in close agreement with those directly measured by  $^{13}\text{C}$  NMR (Table 2). This indicates that the ionization states of Glu78 and Glu172 (free enzyme) primarily dictate the pH dependence of activity in all of the mutant proteins analyzed. In the case of R112N, there is a small discrepancy between the kinetically and NMR determined  $pK_a$  values of Glu78 of 0.5 units which may reflect the scatter in the kinetic data. Nevertheless, the fact that both methods yield very comparable results allows for detailed interpretation of the pH-dependent mechanism of BCX and the electrostatic interplay of Glu78 and Glu172 in catalysis.

**Structures of Mutant BCX Proteins.** The crystal structure of Y69F BCX was solved previously at pH 7.5 to a resolution of 1.5 Å with an *R*-factor of 18.8% (7). The structure was found to be very similar to WT BCX with an overall rms deviation of 0.09 Å for main chain atoms. Hence, the substitution at position 69 had little effect upon the three-dimensional structure of this protein (Figure 6 and Figure S2, Supporting Information). Of the minor changes in the active site of this mutant, a notable case is the shift of Wat A to within hydrogen-bonding distance of Asn35 O $\delta^1$ . Wat A and Wat B (arbitrarily named) are solvent atoms observed

in the active site of BCX proposed to play a role in catalysis (7).

The crystal structure of Y80F BCX was determined at pH 7.5 to a resolution of 1.6 Å with an *R*-factor of 18.1%. The structure showed an overall rms difference of only 0.12 and 0.29 Å for main chain and side chain atoms, respectively, when compared to WT BCX. Most of the changes observed for side chain atoms involved residues located on the surface of the protein. Focusing on the active site of the enzyme, the phenyl ring of the newly introduced Phe80 is shifted relative to Tyr80 in the WT protein as a result of 4° and 9° rotations in the  $\chi_2$  and  $\chi_3$  angles of the side chain, respectively. Other minor changes in the Y80F BCX structure include small rotations in the side chains of Glu172 ( $\Delta\chi_1 = 3^\circ$ ) and Asn35 ( $\Delta\chi_2 = 7^\circ$ ) compared to the WT protein. More notably, Wat B, which is held in place in the free WT enzyme by hydrogen-bonding interactions with Tyr80 O $\eta$  and Gln127 N $\epsilon^2$  (7, 8), is no longer detected in the structure of Y80F BCX. Upon formation of the glycosyl-enzyme intermediate in WT BCX, this water moves to within hydrogen-bonding distance of the general base Glu172 O $\epsilon^2$  and thus appears to act as a nucleophile in the deglycosylation step of the reaction (7). The absence of a corresponding crystallographically identifiable water molecule in Y80F BCX provides a simple explanation for the change in the rate-determining step from glycosylation to deglycosylation with 2,5-DNPX $_2$  as a substrate for this mutant enzyme (discussed later). Wat A, which does not play a role in the second step of the reaction in BCX, is however present.

The structure of Q127A BCX was also determined at pH 7.5 to a resolution of 1.8 Å with an *R*-factor of 16.4%. The overall three-dimensional fold of the protein was retained upon substitution as was evident from a main chain and side chain rms deviation of 0.12 and 0.23 Å, respectively, between Q127A and WT BCX. Changes in the active site of this mutant were confined mostly to the region surrounding the substitution. The position of Glu78 was perturbed as a result of the loss of its interaction with Gln127. Changes of 5° and 7° in  $\chi_1$  and  $\chi_2$ , respectively, were primarily responsible for the movement of Glu78 in toward the cavity created by the alanine substitution at position 127. Also as a consequence of the mutation, a new solvent molecule (Wat C) was found to reside within hydrogen-bonding distance of Glu78 O $\epsilon^1$  (3.1 Å). The loss of a hydrogen-bonding interaction between Gln127 N $\epsilon^2$  and Wat B led to the distance between this water molecule and Glu172 being decreased by 0.7 Å. Another change that surrounded the mutation was a rotation of 10° in the  $\chi_3$  angle of Arg112, bringing the positive charge of its N $\epsilon$  atom 0.5 Å closer to Glu78 O $\epsilon^2$ .

Crystallization trials were performed under a variety of conditions with N35A, R112N, and Q127E BCX, yet were largely unsuccessful. Should the structures of these proteins be obtained at a later date, their coordinates will be deposited in the RCSB Protein Data Bank.

**Structures of WT BCX as a Function of pH.** The structure of WT BCX was solved at apparent pH values of "5.5" and "4.0" to assess the possibility of pH-dependent structural changes within the active site of the enzyme. To perform these studies, crystals were grown at pH 7.5 and transferred to a new buffer at reduced pH. After approximately 4 h was allowed for equilibration, data were collected for each xylanase sample. Thus the exact pH within the crystal was

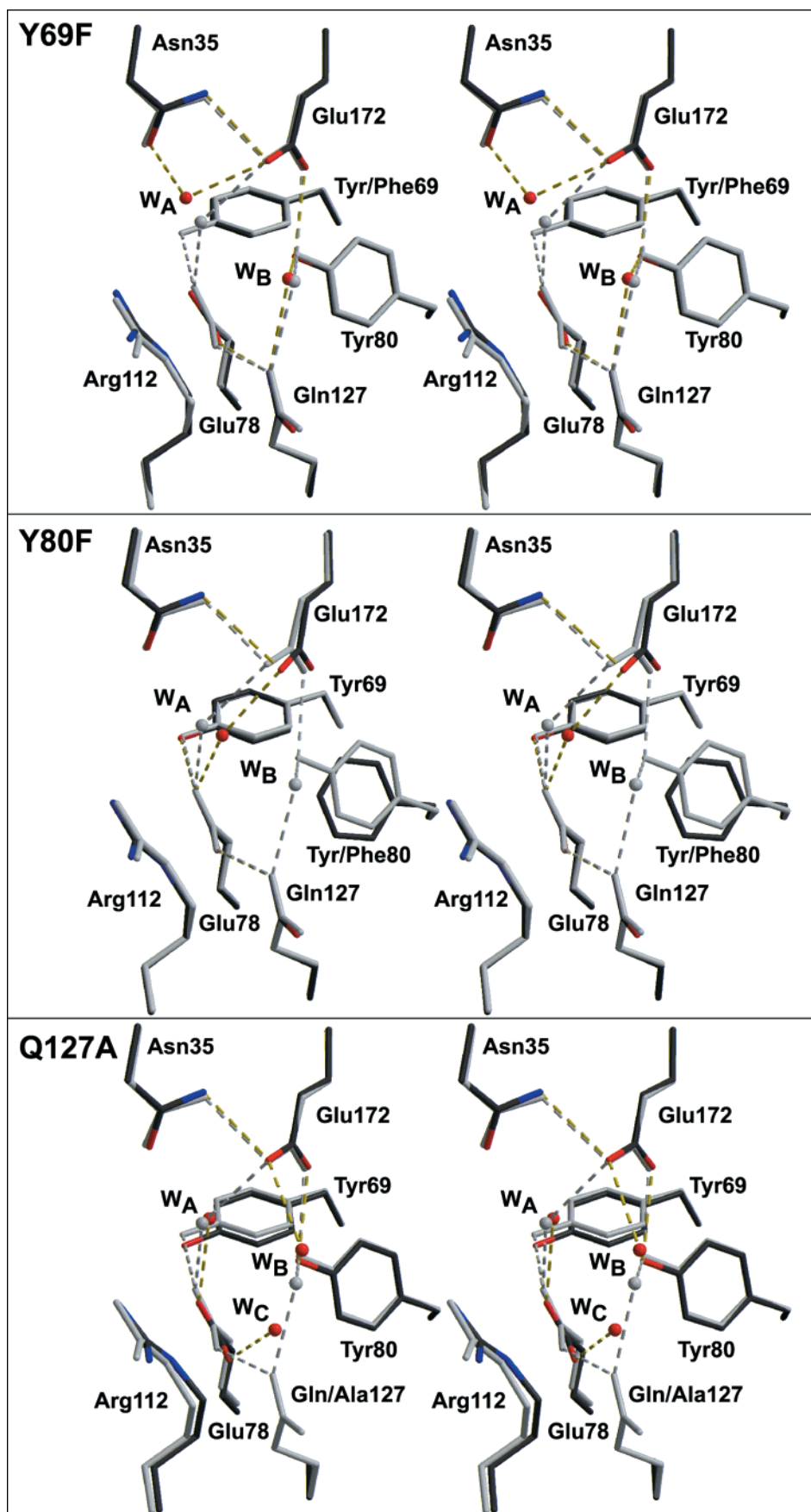


FIGURE 6: Stereo illustrations of the structural conformations of key active site residues of BCX mutants superimposed upon those of the WT protein at pH 7.5. The mutant structures are shown in dark gray, with potential hydrogen bonds indicated by broken yellow lines, protein and water oxygen atoms in red, and nitrogen atoms in blue. The WT reference structure, including all atoms and potential hydrogen bonds, is off-white. See Supporting Information for interatomic distances and rms deviation plots, respectively. Data for Y69F BCX is from ref 7.

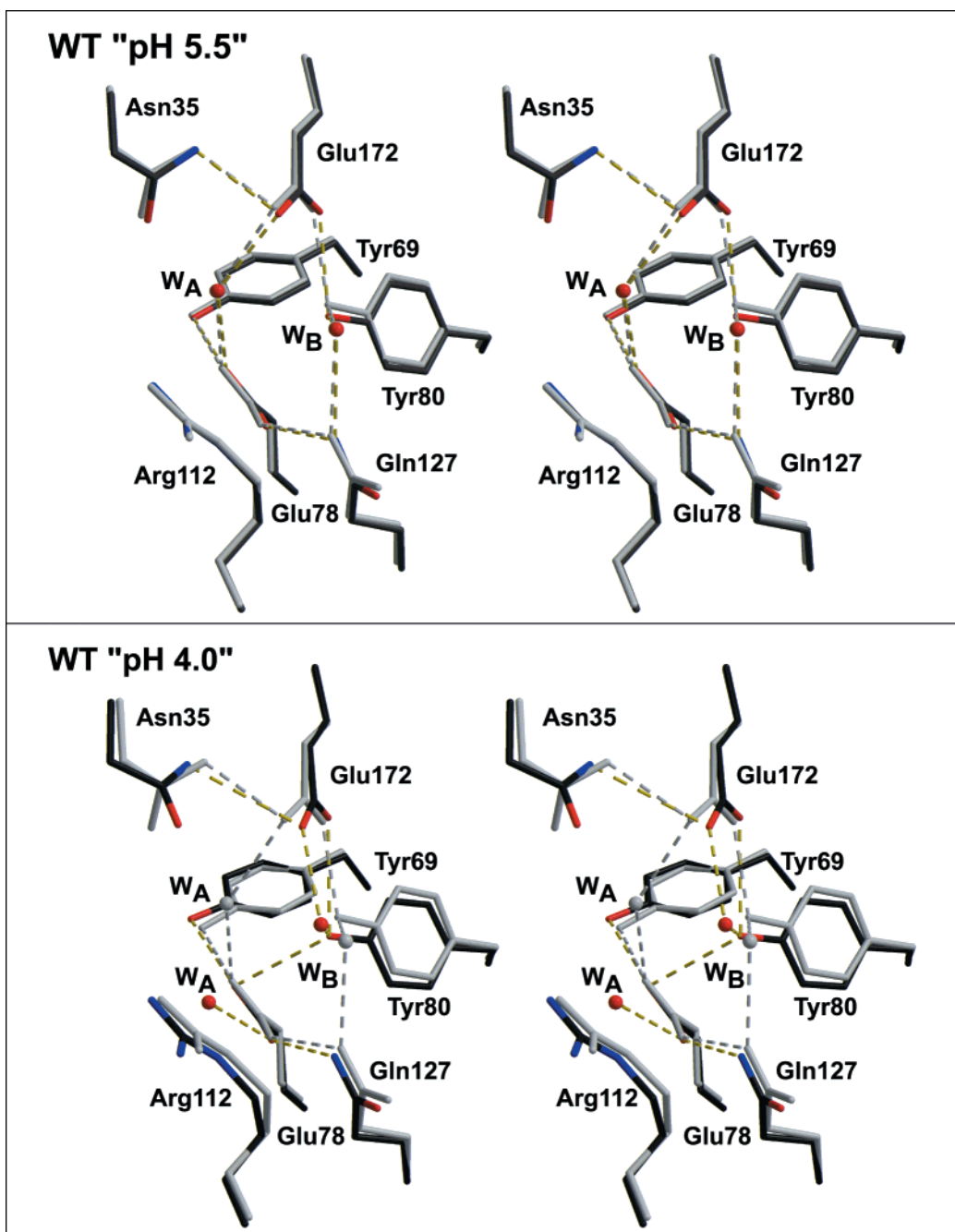


FIGURE 7: Stereo diagrams of the structural conformations of active site residues of WT BCX at apparent pH values of "5.5" and "4.0" superimposed upon those of WT BCX at pH 7.5. The low-pH structures are shown in dark gray, with potential hydrogen bonds indicated by broken yellow lines, protein and water oxygen atoms in red, and nitrogen atoms in blue. The pH 7.5 WT reference structure, including all atoms and potential hydrogen bonds, is off-white. See Supporting Information for interatomic distances and rms deviation plots.

not measured but was assumed to reflect that of the final buffer. This assumption is denoted by the use of quotation marks. The "pH 5.5" structure was determined at a resolution of 1.6 Å with an *R*-factor of 18.4%. The "pH 4.0" structure was determined at a resolution of 1.9 Å with an *R*-factor of 18.0%.

At an apparent pH of 5.5, corresponding to the pH optimum of BCX, virtually no structural changes were present in the active site as evident by a main chain rms difference of 0.08 Å relative to the pH 7.5 WT BCX structure (Figure 7 and Figure S2, Supporting Information). This is somewhat surprising as the ionization state of Glu172 ( $pK_a$  6.7) should differ in the two crystalline states. However,

when the buffer pH was lowered further to 4.0, the main chain rms difference versus the WT increased to 0.15 Å, and the active site showed a number of structural perturbations. In particular, the Asn35 side chain was rotated almost 22° ( $\chi_1$ ) such that it was no longer able to hydrogen bond to Glu172 ( $\Delta\chi_2 = 5^\circ$ ) since the distance between these two residues increased by 0.8 Å to 3.9 Å. The position of the Tyr80 side chain also changed, albeit not so dramatically, such that the hydrogen-bonding distance to the side chain of Glu172 increased from 2.7 to 3.4 Å. Interestingly, the catalytic water (Wat B) proposed to function in the second step of hydrolysis moved almost 2 Å such that it formed stronger hydrogen bonds with both Glu78 (2.6 Å) and

Glu172 (2.9 Å). Note that these changes involve primarily Glu172, rather than Glu78 ( $pK_a$  4.6). This suggests that the pH values of the crystals may have been slightly higher than expected such that Glu172 becomes fully protonated in the lowest pH form while Glu78 remains ionized. In contrast to BCX, in the crystal structure of a family 11 xylanase from *Trichoderma reesei* (XYNII), a notable conformational change is observed for the acid/base catalyst Glu177 when the pH of the crystal is lowered from 6.5 to 4.0 (40). Specifically, the Glu177 side chain flips outward while Tyr88 (analogous to Tyr80 in BCX) changes position such that it can hydrogen bond to the nucleophile Glu86 under conditions of low pH.

**Theoretical  $pK_a$  Calculations.** In addition to the catalytic glutamic acids, the  $pK_a$  values of all remaining carboxyl and imidazole groups in BCX have also been measured (10). Using these reference data, a variety of protocols for theoretical  $pK_a$  calculations were examined. Overall, the best agreement with experimental results was obtained using uniform dielectric constants of 8 and 80 for the protein and solvent, respectively (Table 4). Values of  $pK_a$  calculated (and observed) were Glu78, 2.9 (4.6); Glu172, 5.9 (6.7); Asp4, 3.5 (3.0); Asp11, 2.5 (2.5); Asp83, <0 (<2); Asp101, 0.2 (<2); Asp119, 3.0 (3.2); Asp121, 3.9 (3.6); His149, 3.8 (<2.3); His156, 5.0 (~6.5); and the C-terminal W185, 0.9 (~2.7). Reducing the protein dielectric to 4 yielded a more accurate theoretical  $pK_a$  value of 7.2 for Glu172, yet a poorer value of 2.7 for Glu78. Increasing the protein dielectric to 12 had the opposite effect, giving predicted values of 5.3 for Glu172 and 3.0 for Glu78. The use of a dielectric of 8 for well-ordered residues and 16 for those involved in crystal contacts or with *B*-values higher than 20 (37) produced poorer values for the two glutamic acids, as did explicit inclusion of crystallographically bound waters. Increasing the theoretical ionic strength of the solvent from 0 to 150 mM changed the  $pK_a$  value of Glu78 from 2.4 to 3.4 due to reduced screening of favorable interactions with the positively charged residues in BCX; the increases in the  $pK_a$  values calculated for Glu172 were about half as large due to its titration at higher pH values where the net charge of the protein is less positive.

Although not exact quantitatively, the theoretical and measured  $pK_a$  values for BCX generally agree qualitatively. Notably, abnormally low  $pK_a$  values for Asp83 and Asp101 are predicted. Both residues have  $pK_a$  values below the practical limit of the NMR titrations, indicating that each is always charged within the context of the native enzyme. Structurally, Asp83 is involved in a buried ion pair with Arg136, whereas Asp101 is stabilized in its ionized state by a network of neutral hydrogen-bonding interactions (10). In contrast, one discrepancy is seen with His149, which remains in a neutral state ( $pK_a$  <2.3) under all experimental conditions examined (11). The  $pK_a$  value of this buried residue proved difficult to calculate using an automated protocol as it is hydrogen bonded to an internal water molecule. Inclusion of the water, combined with manual correction of the tautomerization state of His149, reduced the theoretical  $pK_a$  value from 3.8 to <0, thus emphasizing the importance of correctly defining hydrogen-bonding networks with a protein for electrostatic calculations (37). The  $pK_a$  values calculated for the catalytic glutamic acids in the WT and mutant xylanases are summarized in Tables 4 and 5 and will be

Table 4: Theoretically Calculated and Experimentally Measured  $pK_a$  Values in BCX Variants

protein	residue	$pK_a^a$		$\Delta pK_a^b$	
		calcd	obsd	calcd	obsd
WT	Glu78	2.9	4.6		
	Glu172	5.9	6.7		
E78Q	Glu172	4.3	4.2	-1.6	-2.5
E172Q	Glu78	2.8	5.1	-0.1	+0.5
Y69F	Glu78	5.7 <sup>c</sup>	4.9	+2.8 (+1.1) <sup>c</sup>	+0.3
	Glu172	4.3 <sup>c</sup>	8.3	-1.6 (-0.3) <sup>c</sup>	+1.6
Y80F	Glu78	3.1	5.0	+0.2	+0.4
	Glu172	6.2	7.9	+0.3	+1.2
N35A	Glu78	2.6	4.5	-0.3	-0.1
	Glu172	6.1	6.9	+0.2	+0.2
N35D	Glu78	4.0	5.7	+1.1	+1.1
	Glu172	7.5	8.4	+1.6	+1.7
	Asp35	1.0	3.7		
Q127A	Glu78	5.2 <sup>d</sup>	4.2	+2.3 (+0.9) <sup>d</sup>	-0.4
	Glu172	4.8 <sup>d</sup>	7.3	-1.1 (-0.3) <sup>d</sup>	+0.6
Q127E	Glu78	<0	3.8	<-2.9	-0.8
	Glu172	7.3 <sup>e</sup>	6.5	+1.4 (+0.2) <sup>e</sup>	-0.2
	Glu127	5.8 <sup>e</sup>	8.4 <sup>e</sup>		
R112N	Glu78	4.1	5.0	+1.2	+0.4
	Glu172	6.7	7.6	+0.8	+0.9
WT-2FXb	Glu172	3.7	4.2	-2.2	-2.5
N35D-2FXb	Glu172	9.0	1.9-3.4 <sup>f</sup>	+3.1	>-5.0 <sup>f</sup>
	Asp35	0.2 <sup>f</sup>	1.9-3.4 <sup>f</sup>		

<sup>a</sup> Calculated  $pK_a$  values correspond to the pH at which a given residue is 50% ionized (dielectric constants of 8 and 80 for protein and water, respectively; ionic strength of 50 mM, 25 °C). <sup>b</sup>  $\Delta pK_a$  values for the variant are determined by comparison to the corresponding calculated and observed  $pK_a$  values for WT BCX. <sup>c</sup> The calculated titration curves of Glu78 and Glu172 in Y69F are highly biphasic. Fitting the theoretical titration data to a model of two coupled ionizable groups gives microscopic  $pK_a$  values of ~4.0 and ~5.9 for Glu78 in the presence of a neutral or charged Glu172, respectively, and  $pK_a$  values of ~3.7 and ~5.6 for the Glu172 in the presence of neutral or charged Glu78, respectively. For comparison to WT, the corresponding calculated  $\Delta pK_a$  values are for the first microscopic  $pK_a$  of Glu78 ( $\Delta pK_a = +1.1$ ) and the second of Glu172 ( $\Delta pK_a = -0.3$ ). <sup>d</sup> The calculated titration curves of Glu78 and Glu172 in Q127A are highly biphasic and are treated similarly to Y69F (footnote c). Glu78 titrates with microscopic  $pK_a$  values of 3.8 ( $\Delta pK_a = +0.9$ ) and 5.6. Glu172 titrates with microscopic  $pK_a$  values of 3.8 and 5.6 ( $\Delta pK_a = -0.3$ ). <sup>e</sup> The calculated titration curves of Glu127 and Glu172 in Q127E are highly biphasic and are treated similarly to Y69F (footnote c). Glu172 titrates with microscopic  $pK_a$  values of 6.1 ( $\Delta pK_a = +0.2$ ) and 7.4. Glu127 titrates with microscopic  $pK_a$  values of 5.6 and 6.9. <sup>f</sup> Due to strong hydrogen bonding in the covalently modified protein, Asp35-Glu172 titrate as a tightly coupled system with a first  $pK_a$  value in the range of 1.9-3.4 and the second >9 (3).

referred to within the Discussion section.

## DISCUSSION

**Structural Roles of Active Site Residues.** Several highly conserved active site residues are important for the hydrolysis of xylosidic substrates by BCX. Although synthetic substrates with aryl leaving groups that lack interactions with the +1 and beyond subsites were used in this study, the results and trends presented here are consistent with those initially reported in the first major mutational analysis of BCX where the natural substrate xylan was used (8). [According to the nomenclature suggested by Davies et al. (41), cleavage is defined to occur between the -1 and +1 subsites. While natural and synthetic substrates can both form similar interactions with the -2 and -1 subsites on the enzyme, the latter differs with respect to the +1 and beyond subsites due to the presence of a single aryl leaving group instead of

Table 5: Contributions to Theoretically Calculated  $pK_a$  Values in BCX Proteins

protein	residue	caled			
		$pK_a$ value <sup>a</sup>	desolvation <sup>b</sup>	background <sup>b</sup>	ionizable <sup>b</sup>
WT	Glu78	2.9	+2.0	-2.0	-1.5
	Glu172	5.9	+2.3	-1.5	+0.8
E78Q	Glu172	4.3	+2.3	-1.5	-0.9
E172Q	Glu78	2.8	+2.0	-2.0	-1.5
Y69F	Glu78	5.7 <sup>c</sup>	+2.1	-1.0	+0.2
	Glu172	4.3 <sup>c</sup>	+2.0	-1.4	-0.7
Y80F	Glu78	3.1	+1.9	-1.7	-1.5
	Glu172	6.2	+2.0	-1.0	+0.9
N35A	Glu78	2.6	+2.0	-2.2	-1.6
	Glu172	6.1	+2.1	-1.2	+0.8
N35D	Glu78	4.0	+2.3	-2.4	-0.3
	Glu172	7.5	+1.6	-0.9	+2.4
	Asp35	1.0	+1.7	-3.0	-1.7
Q127A	Glu78	5.2 <sup>d</sup>	+2.0	-1.1	-0.1
	Glu172	4.8 <sup>d</sup>	+2.1	-1.5	-0.2
Q127E	Glu78	<0	+2.2	-4.8	>-1.8
	Glu172	7.3 <sup>e</sup>	+2.3	-1.4	+2.0
	Glu127	5.8 <sup>e</sup>	+1.6	-0.9	+0.7
R112N	Glu78	4.1	+1.9	-2.2	-0.1
	Glu172	6.7	+2.2	-1.6	+1.7
WT-2FXb	Glu172	3.7	+1.3	-1.2	-0.9
N35D-2FXb	Glu172	9.0	+2.3	-1.5	+3.8
	Asp35	0.2 <sup>f</sup>	+2.3	-4.2	-1.9

<sup>a</sup> See footnote *a* of Table 4. <sup>b</sup> Contributions to the calculated  $pK_a$  values due to desolvation, interaction with permanent background (partial) charges, and interactions with titratable groups (at pH =  $pK_a$ ), respectively. Model  $pK_a$  values are Asp (4.0) and Glu (4.4). <sup>c</sup> See footnote *c* of Table 4. <sup>d</sup> See footnote *d* of Table 4. <sup>e</sup> See footnote *e* of Table 4. <sup>f</sup> See footnote *f* of Table 4.

a chain of xylose subunits.] For example, Y69F BCX shows no detectable activity on both xylan and ONPX<sub>2</sub>, whereas R112N and Y80F BCX show qualitatively similar but quantitatively different results toward natural and synthetic substrates. Specifically, R112N and Y80F BCX hydrolyze xylan at 12% and ~0.01% of WT levels, respectively, whereas their activities toward the synthetic substrate ONPX<sub>2</sub> are reduced to 4% and 3%, respectively. This difference may reflect additional important interactions between Tyr80 and xylose subunits occurring beyond the site of cleavage (or experimental difficulties in performing assays with less characterizable substrates such as xylan). The nature of such interactions remains to be established as no xylanase structure solved to date contains substrates occupying these subsites (3, 7, 8). Nevertheless, the general reductions in activity seen for the series of mutants on both substrates emphasize the importance of these residues in hydrolysis and the necessity for their absolute conservation among the family 11 xylanases.

Kinetic analyses of mutants of BCX, using well-characterized synthetic substrates, combined with crystallographic structures of these proteins, allow for delineation of the probable functions of the active site residues in these xylanases. The availability of the structure of a catalytically compromised acid/base mutant of BCX reacted with xylo-tetraose (denoted E172C-Xb BCX as only xylobiose is observed in the active site) (8) provides information regarding potential ground state interactions between protein and substrate (Figure 8). In parallel, the more recently solved structure of WT BCX bound to the mechanism-based inhibitor DNP2FXb (WT-2FXb) (7) yields information regarding the glycosyl-enzyme intermediate, including an unusual distortion of the sugar ring in the -1 position that

may facilitate formation of oxocarbenium ion-like transition states for glycosylation and deglycosylation (Figure 8). To a first approximation, changes in  $K_m$  resulting from the mutations studied herein should reflect perturbations in ground state interactions while changes in  $k_{cat}$  would be more related to altered interactions occurring in the transition state. This generalization is not without pitfalls in the case of BCX, however, since the mechanism by which it hydrolyzes xylosidic substrates involves multiple steps.

The side chain of Tyr69 is hydrogen bonded to Glu78. On the basis of the complete inactivity of the Y69F BCX variant, it was initially concluded that Tyr69 might play a role in positioning this nucleophilic glutamate (8). Subsequent elucidation of the crystal structure of Y69F BCX, however, showed nearly exact superposition of active site residues, thus excluding this possibility (7) (Figure 6). However, close structural contacts observed in the WT glycosyl-enzyme intermediate, WT-2FXb, between Tyr69 O<sup>γ</sup> and both Glu78 O<sup>ε2</sup> and the endocyclic oxygen (O5) of the proximal xylose residue in the -1 subsite, indicated a more direct catalytic role for Tyr69 (Figure 6 and Table S3, Supporting Information). Accordingly, it was hypothesized that, through specific charge rearrangements, Tyr69 considerably stabilizes the oxocarbenium ion-like transition state via a direct dipolar interaction between its O<sup>γ</sup> and the partially positively charged O5 atom of the proximal xylose residue. Absence of this crucial interaction in Y69F BCX results in severe crippling of the mutant enzyme.

Tyr80 O<sup>γ</sup> is involved in a hydrogen-bonding interaction with both Glu172 O<sup>ε1</sup> and Wat B (Figure 6). Furthermore, inspection of the crystal structures of WT-2FXb and E172C-Xb shows that Tyr80 O<sup>γ</sup> may interact weakly with the O5 atom of the proximal xylose subunit in the former (distance = 3.6 Å) but not in the latter (distance = 4.6 Å) (Figure 8). Given this difference, Tyr80 may selectively stabilize the proximal saccharide in the transition state and glycosyl-enzyme intermediate relative to the enzyme-substrate complex. Perhaps more importantly, previous studies of WT-2FXb have also revealed that the side chain of Tyr80 helps to position the catalytic water (Wat B) proposed to function as a displacing nucleophile in the deglycosylation step of the hydrolytic reaction. Indeed, an analogous water molecule is not detected in the crystallographic structure of Y80F BCX (7). The apparent absence of this water is consistent with the observation that deglycosylation is the rate-limiting step for hydrolysis of the reactive 2,5-DNPX<sub>2</sub> substrate by this variant xylanase (Figure 4).

In addition to Tyr69, the side chain of Glu78 is hydrogen bonded to the primary amide of Gln127 (O<sup>ε</sup>-N<sup>ε2</sup> distance = 2.7 Å) in the WT enzyme (Figure 6). To probe the role of this interaction, Gln127 was mutated to an alanine and a glutamic acid. The former mutation, Q127A, resulted in the movement of the side chain of Glu78 in toward the cavity formed at the site of substitution. This is the only structure determined where the side chain of Glu78 experiences a positional change, albeit small. An additional bound solvent molecule (Wat C) is also found, satisfying the hydrogen-bonding requirements of the Glu78 carboxylate. Examination of both liganded structures indicates a potential hydrogen-bonding interaction between Gln127 N<sup>ε2</sup> and the O3 atom of the proximal xylose unit (Figure 8). These interactions are weaker (3.5 Å in WT-2FXb and 3.7 Å in E172C-Xb)

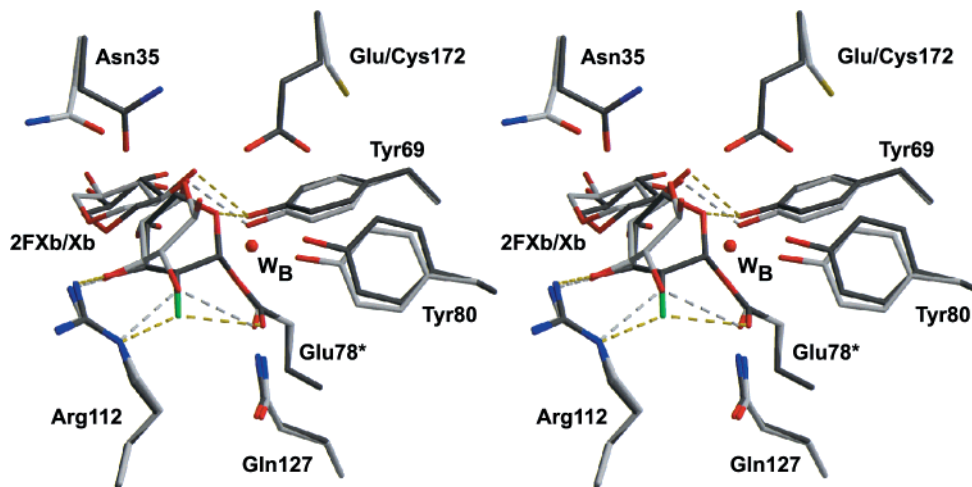


FIGURE 8: A stereo illustration of active site residues of WT-2FXb BCX (dark gray) superimposed upon those of the noncovalent enzyme-substrate complex E172C-Xb BCX (off-white). The former is a trapped covalent glycosyl-enzyme intermediate, whereas the latter is a noncovalent complex of xylootetraose with a catalytically inactive form of the enzyme [only a xylobiosyl unit was observed in the active site cleft (8)]. Potential hydrogen bonds between the enzyme and the saccharide are indicated by broken yellow lines for WT-2FXb and broken off-white lines for E172C-Xb. Oxygen atoms are shown in red, nitrogen atoms in blue, fluorine atoms in green, and sulfur atoms in yellow. The catalytic water ( $W_B$ ) was observed only for WT-2FXb. See Supporting Information for specific interatomic distances.

than those observed for some of the other residues and therefore may not contribute as much to catalysis. However, when combined with the change in position of Glu78, these could easily account for the reduction in activity of Q127A to 11% of WT.

Changing the residue at position 127 to a glutamic acid led to a similar overall reduction in activity to that observed for Q127A BCX. Given that the apparent  $pK_a$  value of Glu127 is  $>6.5$  (Table 3), it must be protonated near the pH optimum of 5.1 measured for this mutant and should resemble the WT glutamine in conformation and hydrogen-bonding potential. No crystal structure was solved, but any structural perturbations of the nucleophile Glu78, which may lead to the observed reductions in  $k_{cat}$  and  $K_m$  due to the amino acid substitution, are likely to be subtle. Alternatively, as discussed below, electrostatic coupling between Glu127 and Glu172 results in a perturbation of the  $pK_a$  of the latter. This in turn may also lead to a change in the activity of the protein, either by altering the ability of Glu172 to serve as a general acid/base catalyst or by changing the population of protein with this residue in its active protonated form (Scheme 2).

The primary amide of Asn35 is involved in a hydrogen-bonding interaction with the carboxyl group of the acid/base catalyst Glu172 (Figure 6). This interaction appears modest, however, as judged both by structure (distance  $O^{\epsilon 2}-N^{\delta 2} = 3.1$  Å) and by the lack of a significant perturbation in the  $pK_a$  value of Glu172 upon its removal by mutation (Table 3). Strikingly, replacement of Asn35 with an Ala leads to a doubling of overall activity of N35A BCX compared to WT as judged by relative  $k_{cat}/K_m$  values. Substitution of an Asp at this site also leads to a 20% increase in activity (3). Thus, these mutations at position 35 are distinct in that they do not impair the catalytic ability of BCX. A possible explanation at least for the reduced  $K_m$  and  $k_{cat}$  values of N35A BCX toward ONPX<sub>2</sub> comes from a comparison of the crystal structures of WT-2FXb and E172C-Xb (Figure 8). In the former (a glycosyl-enzyme intermediate with a distorted proximal sugar) no direct interactions between Asn35 and

the xylose subunits are observed, while in the latter (an inactive enzyme-substrate complex), the side chain of Asn35 is displaced outward. This displacement may be due to the loss of a hydrogen-bonding partner upon substitution of Glu172 by Cys and/or to the avoidance of an unfavorable van der Waals contact with the bound sugar. That is, when the structure of WT BCX is superimposed upon that of E172C-Xb, the distance between Asn35  $O^{\delta 1}$  in the former and the O5 atom of the proximal xylose residue in the latter is 3.2 Å. Thus, in the catalytically competent enzyme-substrate (Michaelis) complex, a potentially destabilizing interaction may exist between Asn35 and the bound substrate. This distance increases to 4.5 Å in WT-2FXb as a result of the proximal sugar adopting a boat conformation. Substitution of an alanine at position 35 would eliminate this contact, thus improving substrate binding to N35A BCX. This would lead to the observed favorable decrease in  $K_m$  yet unfavorable reduction in  $k_{cat}$  (Table 2). Predominance of the latter results in the overall increase in  $k_{cat}/K_m$  relative to the WT enzyme.

Arg112 is positioned approximately equidistant from both Glu78 and Glu172 in the unliganded WT structure and does not make direct contacts with either catalytic residue (Figure 6). In the structures of WT-2FXb and E172C-Xb, however, the side chain of Arg112 is observed to make potential hydrogen-bonding interactions with the O2 (or F2) and O3 atoms of the proximal xylose saccharide (Figure 8). Since these interactions are comparable in the enzyme-substrate complex and glycosyl-enzyme intermediate, we speculate that the significant reduction in the  $k_{cat}$  value of the R112N BCX mutant results from the loss of preferential transition state interactions between Arg112  $N^{\epsilon}$  and the exocyclic oxygens of the proximal saccharide. Interactions of this magnitude are reasonable, since an in-depth study of *Agrobacterium* sp.  $\beta$ -glucosidase has shown that the 2-position of a dinitrophenyl glycoside substrate can contribute almost 4.3 and 5.3 kcal mol<sup>-1</sup> of transition-state binding energy for the glycosylation and deglycosylation steps respectively (24), while interactions at the 3-position can contribute another 2.2 kcal mol<sup>-1</sup> at both transition states.

*pH-Dependent Activity.* With the exception of N35D BCX (3), the pH optima of BCX proteins are set by the  $pK_a$  values of the nucleophile Glu78 and the acid/base catalyst Glu172. That is, the apparent  $pK_a$  values determined from the activity profiles match those determined site-specifically for Glu78 and Glu172 by NMR (Table 2). Hence, the factors that determine the  $pK_a$  values of these two residues dictate the pH-dependent activity of BCX. Any modifications to the local and global environments of Glu78 and Glu172 can result in changes in the pH optimum of the enzyme (summarized in Figure 9).

(i) *Roles of Ionizable Residues.* The presence of ionizable groups in the active site of BCX influences the  $pK_a$  values of both Glu78 and Glu172. Removal of a positive charge contributed by Arg112 resulted in an increase in the pH optimum of the enzyme from 5.7 to 6.2. NMR measurements showed that this shift reflects increases in the  $pK_a$  values of Glu78 and Glu172 by 0.4 and 0.9 unit, respectively (Table 3). This is expected as the positive charge on Arg112 electrostatically stabilizes the conjugate base forms of both Glu residues, thereby serving to lower their  $pK_a$  values relative to that observed with a neutral asparagine at this position. What is less obvious, however, is the greater effect that this mutation has upon the  $pK_a$  of Glu172 compared to Glu78 despite Arg112 being closer to Glu78 by  $\sim 1 \text{ \AA}$  in the crystalline WT enzyme. In the absence of a high-resolution structure of R112N BCX, we must surmise that this reflects the precise microscopic environments of these residues, combined with possible conformational perturbations due to the mutation. In addition, small differences may exist between the structure of BCX in its solution and crystalline forms.

In the case of Q127E BCX, introduction of a Glu residue (Glu127) adjacent to Glu78 serves to *decrease* the pH optimum of this protein from 5.7 to 5.1. This reflects the reduction in  $pK_a$  value of Glu78 by almost 1 unit (the largest observed decrease among the series of active site residue mutants studied herein). However, since the  $pK_a$  of Glu78 is significantly lower than that of Glu127 (Table 3), at its pH optimum, a majority of Q127E BCX molecules are in a state where Glu78 is ionized yet Glu127 is neutral. Hence, Glu127 is protonated and, similar to the WT glutamine, can donate a hydrogen bond to Glu78. Furthermore, the observation that the  $pK_a$  value of Glu78 is 3.8 in the mutant versus 4.6 in the WT enzyme is consistent with the expectation that a neutral glutamic acid can serve as a better hydrogen bond donor than a glutamine due to its greater acidity (42).

In searching for an explanation for the reduced activity of the Q127E BCX mutant, we recognize the need for high-resolution structural data. However, there is no reason to expect that substitution of a glutamic acid for a glutamine would cause significant conformational perturbations in the active site cleft of this protein. It is also unlikely, judging by the WT-2FXb and E172C-Xb structures (Figure 8), that Gln127 makes critical interactions with the substrate. Therefore, we must consider the  $pK_a$  values measured by NMR for the remaining active site carboxyl group in this protein. Due to the lack of a predominant titration step for Glu127 and Glu172 in Q127E BCX, it is difficult to confidently assign  $pK_a$  values to these residues. Following a macroscopic analysis, the observed data can be fitted to yield apparent  $pK_a$  values of 6.5 for Glu172 and  $\sim 8.4$  for Glu127. This

analysis is intuitively correct for three reasons. First, it is consistent with the observation that the basic limb of the pH-dependent activity profile of Q127E BCX, which in all mutants studied herein corresponds to the deprotonation of Glu172, follows an apparent  $pK_a$  value of 6.5. Second, the macroscopic  $pK_a$  value of 8.4, observed for Glu127, can be attributed to electrostatic repulsion from the neighboring Glu78. Finally, with this high  $pK_a$  value, Glu127 remains protonated under most conditions. Thus, position 127 resembles a neutral glutamine, and hence Glu172 has a  $pK_a$  value of 6.5 that is similar to the value of 6.9 measured in the WT enzyme. However, as discussed above, the titration data for the two glutamic acids (Glu127 and Glu172) can be fitted to a branched equilibria model, yielding the microscopic  $pK_a$  values listed in Scheme 2. In the lower ionization pathway of Scheme 2, Glu172 ionizes first with a  $pK_a$  of 6.5, which matches the value observed in the basic limb of the pH-dependent activity profile (Table 2). Since Glu172 is positioned to be the acid catalyst, it must be the group whose deprotonation dictates the alkaline limb of the profile. However, according to Scheme 2, this pathway is followed only  $\sim 50\%$  of the time given the similar values of  $pK_{a1}$  and  $pK_{a2}$ . The other half of the enzyme population is in a state where Glu127 ionizes before Glu172. This would elevate the  $pK_a$  value of Glu172 to 8.5, thereby reducing its ability to serve as a general acid. In the context of this model, this would lower the  $k_{cat}/K_m$  value of Q127E BCX relative to the WT species.

In Joshi et al. (3), we report that the N35D mutation has a profound influence upon the  $pK_a$  values of both the nucleophile and the acid/base catalyst. This mutation is analogous to Q127E in that the amide next to Glu172 is replaced by a carboxyl group. Surprisingly, while this substitution resulted in an *increase* in the  $pK_a$  values of both Glu78 and Glu172 to 5.7 and 8.4, respectively, the pH optimum of the enzyme *decreased* to 4.6. Furthermore, the pH-dependent activity of N35D BCX now followed the  $pK_a$  values of the newly introduced Asp residue ( $pK_a$  3.7) and Glu78 ( $pK_a$  5.7). After extensive analysis, it was determined that Glu78 is still the nucleophile and that Asp35 and Glu172 were functioning together to perform the role of the acid/base catalyst using a "reverse protonation" mechanism (i.e., one in which the  $pK_a$  value of the nucleophile is higher than that of the general acid; 3). In contrast, the pH optimum of Q127E BCX is also reduced due to the introduction of an additional carboxyl group in the active site of the enzyme. In this case, a normal protonation mechanism is followed, and Glu127 does not appear to have any role beyond lowering the  $pK_a$  of Glu78 via hydrogen bonding. These two mutations exemplify two different means by which the pH optima of BCX can be reduced by the presence of an active site carboxyl group.

(ii) *Roles of Neutral Polar Residues.* The mechanisms by which neutral polar residues (i.e., those which do not ionize within the pH range studied) influence the pH-dependent activity of BCX appear to be more subtly manifested. Removal of a hydrogen bond to Glu172 contributed by Asn35 was achieved through substitution of this residue by an Ala. The mutation resulted in no change in the pH optimum of the enzyme nor any perturbations in the  $pK_a$  values of Glu78 and Glu172. While understandable for the distal Glu78, this observation is somewhat unexpected for

Table 6: Average Hydrogen-Bonding Distances and Acceptor Angle Deviations Observed for Glu78 and Glu172 in All BCX Proteins

interaction	donor type	average distance (Å) <sup>a</sup>	average acceptor angle deviation (deg) <sup>a,b</sup>	$\Delta pK_{a\text{Glu78}}^c$	$\Delta pK_{a\text{Glu172}}^c$
Glu78 O <sup>ε1</sup> –Gln127 N <sup>ε2</sup>	NH <sub>2</sub>	2.7	33	−0.4	+0.6
Glu172 O <sup>ε2</sup> –Asn35 N <sup>δ2</sup>	NH <sub>2</sub>	3.4	4	−0.1	+0.2
Glu78 O <sup>ε2</sup> –Tyr69 O <sup>γ</sup>	OH	2.7	15	+0.3	+1.6
Glu172 O <sup>ε1</sup> –Tyr80 O <sup>γ</sup>	OH	2.9	4	+0.4	+1.2

<sup>a</sup> Structural coordinates used for average value of distance/angle measurements were obtained from the RCSB Protein Data Bank (31), PDB identification number 1XNB for WT BCX at pH 7.5 (8), 1BVV for WT-2FXB BCX at pH 7.5 (7), and 2BVV for Y69F BCX (7). Structures that were used from this study include WT BCX at pH 5.5, WT BCX at pH 4.0, Y80F BCX (1HV0), and Q127A BCX (1HV1). <sup>b</sup> Hydrogen bond acceptor angles (C<sup>δ</sup>–O<sup>ε1/2</sup>...X) and distances of Glu78 and Glu172 were measured using heavy atom positions. The ideal acceptor angle for a Glu/Asp side chain carboxyl group is 120° (50). Deviations (absolute values) were calculated by subtracting the ideal angle from the measured angle. <sup>c</sup>  $\Delta pK_a = pK_a(\text{mutant}) - pK_a(\text{WT})$  (differences were calculated using the major  $pK_a$  values of the respective mutant and WT; e.g., for the Glu78 O<sup>ε1</sup>–Gln127 N<sup>ε2</sup> interaction, the  $\Delta pK_a$  value listed is for Q127A BCX where Gln127 is removed).

Glu172. However, the interaction between Asn35 and Glu172 may be relatively weak (distance Asn35 N<sup>δ2</sup> to Glu172 O<sup>ε2</sup> = 3.1 Å), suggesting that the asparagine contributes little to the relative stability of the neutral versus ionized state of its neighboring glutamic acid. Consistent with this notion, the position of Asn35 also varies in several of the BCX structures solved (Y80F, WT “pH 4.0”, E172C-Xb BCX; Tables S1 and S2, Supporting Information), implying a degree of structural flexibility at this site. Alternatively, it is possible that a new solvent molecule occupies the cavity created by mutation of the asparagine side chain to an alanine, thereby providing a compensating hydrogen bond to maintain the  $pK_a$  value of Glu172.

Surprisingly, removal of the hydrogen bond contributed by Gln127 to the nucleophile Glu78 influenced the  $pK_a$  values of both catalytic residues. That is, the  $pK_a$  value of Glu78 decreased from 4.6 to 4.2 while that of Glu172 increased from 6.7 to 7.3 when Gln127 was mutated to an Ala. This resulted in a broadening of the pH–activity profile of Q127A BCX without a significant shift in its pH optimum. The reduced  $pK_a$  observed for Glu78 is unexpected as removal of the hydrogen bond from Gln127 should lead to the opposite effect. It is possible that a new solvent molecule (Wat C in Figure 6), observed in the structure of Q127A BCX to occupy the position corresponding to the Gln127 side chain in WT BCX, serves to stabilize better the ionized form of Glu78. At the same time, removal of the glutamine side chain may expose Glu78 to the high dielectric and ionic environment of the solvent, thus reducing the unfavorable Born energy due to partial burial of this residue. (However, this is not predicted by our electrostatic calculations; Table 5.) Given the localized structural perturbations resulting from the Q127A mutation, there is also no obvious explanation for the precise nature by which the mutation leads to an increase in the  $pK_a$  value of Glu172 by 0.5 units. It is possible that this change reflects subtle alterations in the complex hydrogen-bonding network within the active site of BCX.

The side chain of Tyr80 is positioned such that it can donate a hydrogen bond to Glu172 at pH 7.5. Removal of this hydrogen bond by mutation to a Phe results in an increase in the pH optimum of BCX from 5.7 to 6.3, due to elevation of the apparent  $pK_a$  values of Glu78 and Glu172 from 4.6 to 4.8 and 6.7 to 7.7, respectively. The latter result is expected on the basis of the structure of BCX, in which the side chain of Tyr80 clearly contributes a charge-stabilizing hydrogen bond to Glu172. The smaller increase in the  $pK_a$  value of Glu78 upon mutation of Tyr80 to Phe can be rationalized by examination of the structure of WT

BCX at “pH 4”. At this lowered pH, the side chain of Tyr80 shifts slightly such that it can weakly hydrogen bond with either Glu78 O<sup>ε1</sup> or O<sup>ε2</sup> (distance Tyr80 O<sup>γ</sup> to Glu78 O<sup>ε1</sup> or O<sup>ε2</sup> = 3.4 Å), while still interacting with the presumably neutral Glu172 O<sup>ε1</sup>. In this manner, Tyr80 can hydrogen bond to both Glu78 and Glu172 as required. The dynamic hydrogen-bonding ability of Tyr80 likely reflects its ability to function as both a hydrogen bond acceptor and donor and thereby adapt to accommodate pH-dependent changes that occur in the active site of BCX.

The side chain of Tyr69 forms a strong hydrogen bond to the side chain of Glu78. When this interaction is removed through mutation of Tyr69 to Phe, the  $pK_a$  of Glu78 rises by 0.3 units to 4.9. Unexpectedly, the  $pK_a$  of Glu172 increases by 1.6 units to a value of 8.3. The pH optimum of the enzyme was not measurable, since the Y69F mutant is inactive. As seen for other BCX mutants, the  $pK_a$  value of Glu172 is more sensitive to changes in the active site than is the  $pK_a$  of Glu78. It is clear that the strong hydrogen bond between Tyr69 and Glu78 can serve to lower the  $pK_a$  of this nucleophilic residue. However, the mode by which Tyr69 lowers the  $pK_a$  of Glu172 is less obvious since the O<sup>γ</sup> atom of this tyrosine is >5 Å away from either Glu172 O<sup>ε2</sup> or O<sup>ε1</sup>. Unlike Tyr80, the position of the side chain of Tyr69 does not change with pH such that it can form a hydrogen bond with Glu172. As mentioned previously, however, the ionizations of Glu78 and Glu172 are electrostatically coupled, and via this linkage the changes in the  $pK_a$  of one partner can influence the ionization of the other. Furthermore, it is interesting to note that Tyr69 and Tyr80 stack in a typical T-shaped or edge-to-face stacking interaction arrangement with their closest inter-side-chain distance being 3.6 Å (Tyr69 C<sup>δ1</sup> to Tyr80 C<sup>ε2</sup>), which is well within the prescribed range for such aromatic–aromatic interactions (43). This interaction may provide an additional avenue by which the  $pK_a$  value of Glu172 is perturbed by the substitution of Tyr69 by Phe.

(iii) *Hydrogen Bonding.* The degree to which a specific hydrogen bond can influence the  $pK_a$  values of Glu78 and Glu172 is dependent on the length of the bond and the identity of the donor (Table 6). Removal of hydrogen-bonding residues generally serves to raise the  $pK_a$  values of the catalytic glutamic acids and hence the pH optimum of the enzyme. Mutation of residues that donate shorter and therefore stronger hydrogen bonds to Glu78 and Glu172 results in larger perturbations in  $pK_a$  values. However, no trend was observed between the ideality of the hydrogen bond donor angle and its influence on  $pK_a$  value.

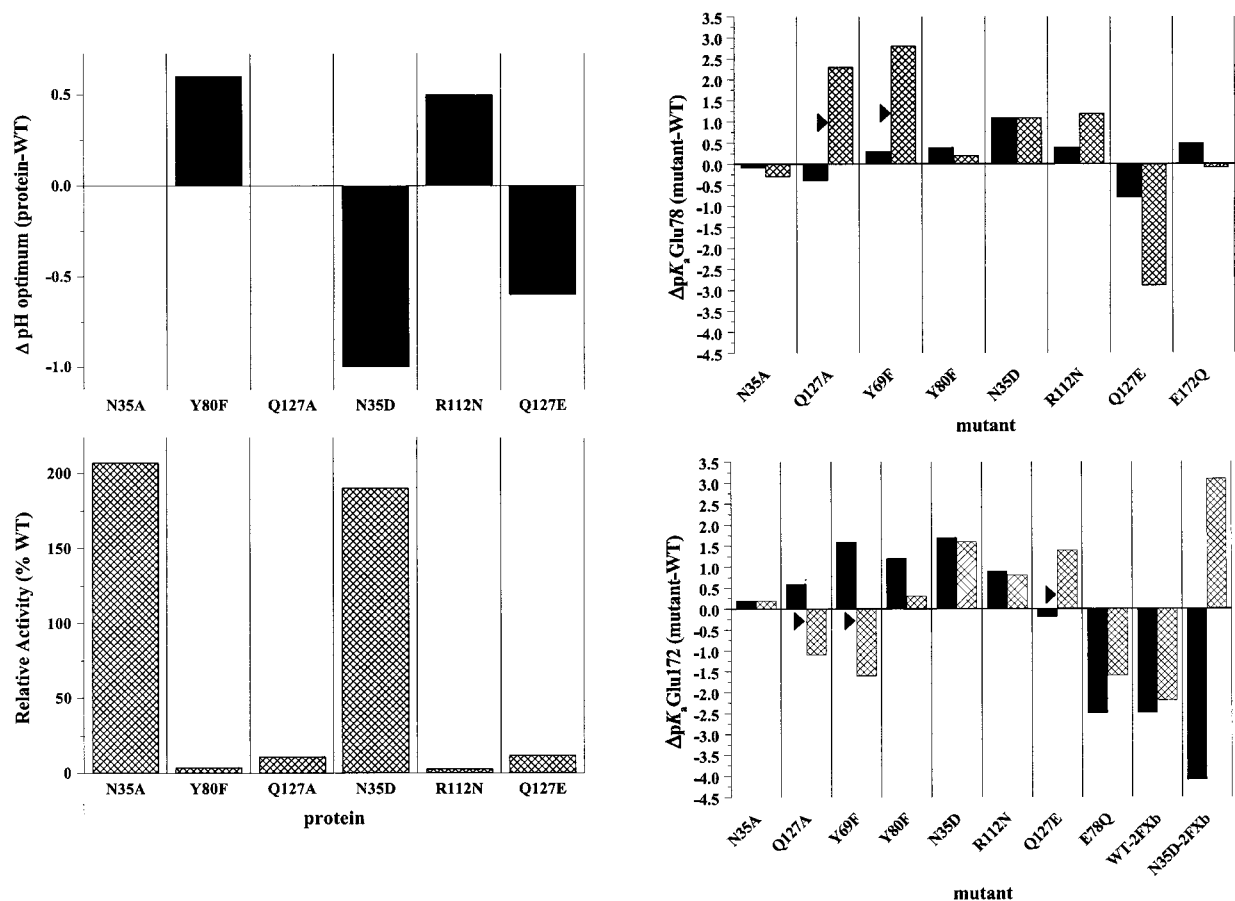


FIGURE 9: Summary of the effects of active site substitutions. Changes in pH optimum (upper left) are indicated relative to the WT value of 5.7 using data obtained from activity profiles (Table 2). Activity levels (lower left) are shown relative to WT (100%) and were determined on the basis of the parameter  $k_{cat}/K_m$  (Table 2). Changes in the  $pK_a$  values of Glu78 (upper right) and Glu172 (lower right) based on experimental NMR data (solid) or calculated theoretical values (hatched) are shown. In cases of calculated titration curves that are highly biphasic, the predicted microscopic  $\Delta pK_a$  values (rather than 50% ionization point), derived with the interacting carboxyl in the appropriate ionization state, are indicated by an arrowhead symbol (Table 4). With N35D-2FXb, the observed  $\Delta pK_a$  corresponds to the first ionization of the Asp35-Glu172 pair, whereas the calculated  $\Delta pK_a$  reflects Glu172 treated as an independent carboxylic acid (3). Differences are plotted using only NMR data (solid = NMR  $pK_a$  mutant – NMR  $pK_a$  WT) or only calculated data (hatched = calculated  $pK_a$  mutant – calculated  $pK_a$  WT) (Table 4).

The chemical identity of the hydrogen bond donor is also a factor that can dictate  $pK_a$  values of residues 78 and 172. Energies of hydrogen bonds between uncharged donors and uncharged acceptors range from 0.5 to 1.5 kcal mol<sup>-1</sup>, whereas those involving one charged group in the pair are larger at ~3.5–4.5 kcal mol<sup>-1</sup> (44). On the basis of simple electrostatic models, the energy of a hydrogen bond reaches a maximum value when  $\Delta pK_a = 0$  between donor and acceptor (45). In nonprotic solvents, it is estimated that each pH unit of mismatch between donor and acceptor weakens the hydrogen bond by a factor of 5 (46, 47). On the basis of  $pK_a$  values determined from model compounds (48), the order of the strengths of hydrogen bonds should, to a first approximation, follow the trend Glu-Glu/Asp (COOH) > Glu-Tyr (OH) > Glu-Gln/Asn (CONH<sub>2</sub>). Consistent with this trend, we find that hydrogen bonds donated by neutral Glu/Asp residues (Glu127 in Q127E) lower the  $pK_a$  values of the catalytic glutamic acids the most, followed next by Tyr residues (Tyr69 and Tyr80 in WT BCX) and finally by Gln/Asn residues (Asn35 and Gln127 in WT BCX) (6).

As mentioned above, the  $pK_a$  of Glu172 is markedly more sensitive to active site substitution compared to that of Glu78 (Figure 9). Inspection of Table 6 shows that Glu78 is flanked by two very well ordered residues (Tyr69 and Gln127) whose

hydrogen-bonding distances remain short (2.7 Å) in all proteins studied. In contrast, hydrogen bond donors to Glu172 are not as rigidly placed (Asn35 and Tyr80), as judged by the variation in interatomic distances for the series of mutant structures (Tables S1 and S2, Supporting Information). Normalized isotropic thermal factors are also consistently higher for Glu172 and the residues surrounding it when considering all of the BCX structures examined in this study. Together, these potential dynamic differences may account for the greater degree of charge stabilization afforded to Glu78 and contribute to its  $pK_a$  being lower than Glu172. This behavior can be rationalized when considering the functions of Glu78 and Glu172. Glu78 must be positioned rigidly as a negatively charged nucleophile for the first crucial step of hydrolysis. In contrast, Glu172 performs dual functions as a general acid and base and must be accommodated in the active site in either a protonated or deprotonated state. This requires that it be positioned to protonate the leaving aglycon in the first step and be held in proximity to a nucleophilic water molecule for the second step.

*Theoretical  $pK_a$  Calculations.* Within the context of this study, we were particularly interested in the calculated  $pK_a$  values for Glu78 and Glu172 in the free WT enzyme. These two catalytic glutamic acids are in very similar hydrogen-

bonding environments with comparable degrees of solvent exposure, thus requiring a detailed analysis to explain their different ionization behaviors. As summarized in Table 5, electrostatic calculations indicate that Glu78 has a slightly less unfavorable desolvation energy than Glu172 (+2.0 vs +2.3 pK<sub>a</sub> units), combined with more favorable background interactions involving the permanent partial charges of the protein (-2.0 vs -1.5 pK<sub>a</sub> units). Together, these shift the "intrinsic" pK<sub>a</sub> [that is, the pK<sub>a</sub> in the absence of interactions with any titratable groups; (38)] of Glu78 below that of Glu172. Consideration of favorable interactions with surrounding ionizable groups reduces the pK<sub>a</sub> of Glu78 by a further -1.5 units to a final calculated value of 2.9. These interactions involve primarily Arg112 (-1.2 units, as indicated by the effects of removing this positive charge in the R112N mutant), compounded by contributions from the net global positive charge of BCX at acidic pH values. The reason as to why the calculated pK<sub>a</sub> of 2.9 for Glu78 differs from the measured value of 4.6 is not clear, although this may reflect an inadequate description of the microscopic environment (solvation and dielectric constant) along the surface of the active site or subtle differences between the structure of the protein in solution and in a crystalline environment due to side chain and backbone mobility (49).

Combined with the calculation of a lower intrinsic pK<sub>a</sub> for Glu78 relative to Glu172, the most salient aspect of the electrostatic calculations is that the glutamic acids are strongly coupled with an unfavorable charge-charge interaction of 1.6 units. Thus, with rising pH, Glu78 predominantly deprotonates first, thereby disfavoring the ionization of Glu172 and elevating its pK<sub>a</sub> to a calculated value of 5.9. Thus, the large difference in the apparent pK<sub>a</sub> values of Glu78 and Glu172 results intrinsically from their electrostatic juxtaposition within the active site of the enzyme. This key conclusion is supported both experimentally (6; Figure S1, Supporting Information) and theoretically (M. D. Joshi, J. E. Nielsen, and L. P. McIntosh, in preparation) by the observation and prediction, respectively, of biphasic titration curves reflecting the coupled microscopic ionization behavior of these two residues. In addition, paralleling that observed experimentally, the calculated pK<sub>a</sub> of Glu172 in the E78Q mutant decreases by 1.6 units to 4.3 due to removal of the negative charge at position 78 (Table 6). (Conversely, the pK<sub>a</sub> of Glu78 in E172Q BCX is essentially unperturbed relative to the WT enzyme since, in both cases, it corresponds to ionization in the presence of a neutral residue at 172.) Covalent modification of Glu78 to form the glycosyl-enzyme intermediate, WT-2FXb BCX, also results in a similar decrease in the predicted pK<sub>a</sub> value of Glu172 to 3.7 due to the removal of charge repulsion, as well as smaller changes in desolvation and background interaction energies (Table 5). This supports the previous conclusion that "cycling" of the pK<sub>a</sub> value of Glu172 to match its role as a general acid and then base during the two-step double-displacement reaction results *intrinsically* from the cycling of the nucleophile between its charged carboxylate and neutral glycosylated states (6).

Theoretical pK<sub>a</sub> calculations were also carried out for several variants of BCX (Tables 4 and 5). Figure 9 presents a summary of these results, emphasizing the changes in the pK<sub>a</sub> values predicted for the catalytic glutamic acids rather than their absolute values. Inspection of these data reveals a

general agreement with that measured experimentally. In particular, the theoretical calculations indicated that removal of hydrogen-bonding interactions and favorable positive charges, as well as the introduction of unfavorable negative charges, leads to the elevation of the pK<sub>a</sub> values predicted for Glu78 and Glu172. This is in accord with that expected from simple electrostatic considerations. In several cases, such as that of Y69F BCX, the changes in the calculated pK<sub>a</sub>, based on a definition of 50% ionization, were overestimated. Inspection of the predicted curves of fractional ionization versus pH revealed highly biphasic titrations (not shown). Extraction of microscopic pK<sub>a</sub> values, corresponding to the situation in which the interacting carboxyl is in the ionization state expected, reduced the magnitude of the predicted changes to better match the experimentally observed results (see footnotes to Table 4).

Closer inspection of the data shown in Figure 9 indicates that the direction and magnitude of the change in pK<sub>a</sub> upon mutation are more accurately predicted for the removal/addition of ionizable residues (N35D, R112N, Q127E, E78Q, E172Q, and WT-2FXb) in proximity to Glu78 and Glu172 than they are for the mutation of nonionizable residues that donate hydrogen bonds (N35A, Q127A, Y69F, and Y80F) to the catalytic pair. The theoretical calculations also do not predict the marked sensitivity of the pK<sub>a</sub> of Glu172 to active site substitution compared to Glu78. The differences between the measured and predicted pK<sub>a</sub> values, in this regard, reflect the need to define accurately the precise geometry of hydrogen bond networks and proton placement, as well as to consider the effects of explicit interactions with solvent molecules. Furthermore, as discussed previously, many additional factors, such as pH-dependent changes in structure (Figure 7) or dynamics, which may not be accounted for by computational methods, can also serve to influence the ability of a donated hydrogen bond to stabilize/destabilize the pK<sub>a</sub> of an ionizable group.

## CONCLUSION

The three-dimensional structure of BCX has been finely tuned at the local and global levels to not only maintain the correct ionization states of the catalytic glutamic acids but also position active site residues for catalytically optimal protein-substrate interactions. The active site residues act concertedly in setting the pK<sub>a</sub> values of Glu78 and Glu172, with no particular group being singly more important than any of the others. As a result of the intricate network of van der Waals, hydrogen-bonding and electrostatic interactions, both catalytic glutamic acid residues are perturbed in complex ways upon active site substitution. In general, positively charged groups serve to lower pK<sub>a</sub> values as do residues that contribute hydrogen bonds. The length of the hydrogen bond and the chemical identity of the donor are also factors dictating the degree of charge stabilization afforded to the ionizable acceptor. Groups that donate shorter hydrogen bonds are more effective in lowering pK<sub>a</sub> values than those that contribute longer hydrogen bonds. In contrast, the mechanism by which adjacently positioned acidic residues lower pK<sub>a</sub> values is more complex and is dependent upon the electrostatic linkage of the groups involved in the interaction. In the case of BCX, substitutions of carboxyl groups near the nucleophile (Q127E) and the acid/base catalyst (N35D) both resulted in lower pH optima; however,

this net effect was accomplished via dramatically different mechanisms.

Complementing these experimental results, theoretical  $pK_a$  calculations provide qualitative insights into electrostatic interactions occurring in BCX. In particular, a key conclusion from these calculations is that the high apparent  $pK_a$  value of Glu172 results from unfavorable electrostatic interactions with Glu78, which has a lower intrinsic  $pK_a$  due to global stabilization by background (partial) and titratable charged groups, combined with lower desolvation energies.

In most cases, mutation of active site residues also leads to significant reductions of activity. This is not surprising since these groups are involved in ground and/or transition state binding of the saccharide. Active site substitutions generally lead to small structural perturbations yet can significantly alter activity, including the rate-determining step and pH dependence of hydrolysis. Thus, while the pH optimum of BCX can be modified from  $-1.1$  to  $+0.6$  pH units, this generally occurs at the expense of activity. Strategies for engineering pH optima of enzymes can involve mutations of key active site residues. However, more general approaches would likely involve changing residues outside the core of the active site to avoid perturbing the exquisitely balanced network of complex interactions that surround these catalytic groups. In this manner, longer range electrostatic interactions could be taken advantage of to perturb the  $pK_a$  values of ionizable active site residues and hence shift the pH optimum of an enzyme. Mechanistic considerations are also central to successful engineering of glycosidases. For example, further studies are necessary to probe the effects that alterations have upon phenomena such as  $pK_a$  cycling as well as the ionization behavior of key residues in the transition states of these enzymatically catalyzed reactions.

## ACKNOWLEDGMENT

We thank Dr. Shouming He for assistance with electro-spray mass spectrometry studies, David Zechel for synthesizing various substrates, Dr. Robert Maurus and Nham Nguyen for crystallographic assistance, and Dr. Warren Wakarchuk and Dr. Rebecca Wade for helpful discussions. We dedicate this paper to the memory of our colleague, Dr. Michael Smith, and his unwavering support of basic scientific research.

## SUPPORTING INFORMATION AVAILABLE

Three tables, S1, S2, and S3, listing salient interatomic distances for mutant, WT, and substrate-bound BCX proteins, respectively, Figure S1 showing resulting coupled ionization schemes for WT, N35A, Y69F, and Q127A BCX proteins (similar to Scheme 2 for Q127E BCX), and Figure S2 showing the rms deviations of main chain and side chain heavy atoms of Y80F, Q127A, and WT BCX at apparent pH values of 5.5 and 4.0, compared to the WT species at pH 7.5. This material is available free of charge via the Internet at <http://pubs.acs.org>.

## REFERENCES

- Sung, W. L., Luk, C. K., Zahab, D. M., and Wakarchuk, W. (1993) *Protein Expression Purif.* 4, 200–206.
- Wakarchuk, W., Methot, N., Lanthier, P., Sung, W., Seligy, V., Yaguchi, M., To, R., Campbell, R., and Rose, D. (1992) in *Xylan and xylanases* (Visser, J., et al., Eds.) pp 439–442, Elsevier Science B. V., Amsterdam.
- Joshi, M. D., Sidhu, G., Pot, I., Brayer, G. D., Withers, S. G., and McIntosh, L. P. (2000) *J. Mol. Biol.* 299, 255–279.
- Lawson, S. L., Wakarchuk, W. W., and Withers, S. G. (1996) *Biochemistry* 35, 10110–10118.
- Lawson, S. L., Wakarchuk, W. W., and Withers, S. G. (1997) *Biochemistry* 36, 2257–2265.
- McIntosh, L. P., Hand, G., Johnson, P. E., Joshi, M. D., Komer, M., Plesniak, L. A., Ziser, L., Wakarchuk, W. W., and Withers, S. G. (1996) *Biochemistry* 35, 9958–9966.
- Sidhu, G., Withers, S. G., Nguyen, N. T., McIntosh, L. P., Ziser, L., and Brayer, G. D. (1999) *Biochemistry* 38, 5346–5354.
- Wakarchuk, W. W., Campbell, R. L., Sung, W. L., Davoodi, J., and Yaguchi, M. (1994) *Protein Sci.* 3, 467–475.
- Plesniak, L. A., Wakarchuk, W. W., and McIntosh, L. P. (1996) *Protein Sci.* 5, 1118–1135.
- Joshi, M. D., Hedberg, A., and McIntosh, L. P. (1997) *Protein Sci.* 6, 2667–2670.
- Plesniak, L. A., Connelly, G. P., Wakarchuk, W. W., and McIntosh, L. P. (1996) *Protein Sci.* 5, 2319–2328.
- Gilkes, N. R., Henrissat, B., Kilburn, D. G., Miller, R. C., Jr., and Warren, R. A. (1991) *Microbiol. Rev.* 55, 303–315.
- Koshland, D. E. (1953) *Biol. Rev.* 28, 416–436.
- Sinnott, M. L. (1990) *Chem. Rev.* 90, 1171–1202.
- Gebler, J., Gilkes, N. R., Claeysens, M., Wilson, D. B., Béguin, P., Wakarchuk, W. W., Kilburn, D. G., Miller, R. C., Jr., Warren, R. A., and Withers, S. G. (1992) *J. Biol. Chem.* 267, 12559–12561.
- Miao, S., Ziser, L., Aebersold, R., and Withers, S. G. (1994) *Biochemistry* 33, 7027–7032.
- Kunkel, T. A., Roberts, J. D., and Zakour, J. (1983) *Methods Enzymol.* 154, 367–382.
- Muchmore, D. C., McIntosh, L. P., Russell, C. B., Anderson, D. E., and Dahlquist, F. W. (1989) *Methods Enzymol.* 177, 44–73.
- Anderson, D. E., Lu, J., McIntosh, L. P., and Dahlquist, F. W. (1993) in *NMR of Proteins* (Clare, G. M., and Gronenborn, A. M., Eds.) pp 258–304, Macmillan Press, London.
- Ziser, L., Setyawati, I., and Withers, S. G. (1995) *Carbohydr. Res.* 274, 137–153.
- Leatherbarrow, R. J. (1998) *Gra-Fit, Version 4.0*, Erithacus Software Ltd., Staines, U.K.
- Zechel, D. L., Konermann, L., Withers, S. G., and Douglas, D. J. (1998) *Biochemistry* 37, 7664–7669.
- Hiroimi, K. (1979) *Kinetics of fast enzyme reactions*, John Wiley & Sons, New York.
- Namchuk, M. N., and Withers, S. G. (1995) *Biochemistry* 34, 16194–16202.
- Shrager, R. I., Cohen, J. S., Heller, S. R., Sachs, D. H., and Schechter, A. N. (1972) *Biochemistry* 11, 541–547.
- Otwinowski, Z., and Minor, W. (1997) *Methods Enzymol.* 276, 307–326.
- Brunger, A. T. (1992) *X-PLOR version 3.1: A system for X-ray crystallography and NMR*, Yale University Press, New Haven, CT.
- Collaborative Computational Project Number 4 (1994) *Acta Crystallogr.* D50, 760–763.
- Jones, T. A., Zhou, J. Y., Cowan, S. W., and Kjeldgaard, M. (1991) *Acta Crystallogr.* A47, 110–119.
- Luzzati, P. V. (1952) *Acta Crystallogr.* A50, 803–810.
- Berman, H. M., Westbrook, J., Feng, Z., Gilliland, G., Bhat, T. N., Weissig, H., Shindyalov, I. N., and Bourne, P. E. (2000) *Nucliec Acids Res.* 28, 235–242.
- Kraulis, P. J. (1991) *J. Appl. Crystallogr.* 24, 946–950.
- Merrit, E. A., and Murphy, M. E. (1994) *Acta Crystallogr.* D50, 869–873.
- McDonald, I. K., and Thornton, J. M. (1994) *J. Mol. Biol.* 238, 777–793.
- Hoof, R. W. W., Sander, C., and Vriend, G. (1996) *Proteins* 26, 363–376.

36. Nielsen, J. E., Beier, L., Otzen, D., Borchert, T. V., Frantzen, H. B., Andersen, K. V., and Svendsen, A. (1999) *Eur. J. Biochem.* 264, 816–824.
37. Nielsen, J. E., and Vriend, G. (2001) *Proteins* 43, 403–412.
38. Yang, A., and Honig, B. (1993) *J. Mol. Biol.* 231, 459–474.
39. Tull, D., and Withers, S. G. (1994) *Biochemistry* 33, 6363–6370.
40. Törrönen, A., and Rouvinen, J. (1995) *Biochemistry* 34, 847–856.
41. Davies, G. J., Wilson, K. S., and Henrissat, B. (1997) *Biochem. J.* 321, 557–559.
42. Stahl, N., and Jencks, W. P. (1986) *J. Am. Chem. Soc.* 108, 4196–4205.
43. McGaughey, G. B., Gagne, G., and Rappe, A. K. (1998) *J. Biol. Chem.* 273, 15458–15463.
44. Fersht, A. R., Shi, J. P., Knill-Jones, J., Lowe, D. M., Wilkinson, A. J., Blow, D. M., Brick, P., Carter, P., Waye, M. M., and Winter, G. (1985) *Nature* 314, 235–238.
45. Shan, S. O., Loh, S., and Herschlag, D. (1996) *Science* 272, 97–101.
46. Shan, S., and Herschlag, D. (1996) *Proc. Natl. Acad. Sci. U.S.A.* 93, 14474–14479.
47. Cleland, W. W., and Northrop, D. B. (1999) *Methods Enzymol.* 308, 3–27.
48. Kyte, J. (1994) *Structure in protein chemistry*, Garland Publishing, New York and London.
49. Connelly, G. P., Withers, S. G., and McIntosh, L. P. (2000) *Protein Sci.* 9, 512–524.
50. Jeffrey, G. A., and Saenger, W. (1991) *Hydrogen Bonding in Biological Structures*, Springer-Verlag, Berlin.

BI0105429